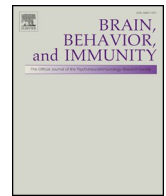




Contents lists available at ScienceDirect

Brain, Behavior, and Immunity

journal homepage: www.elsevier.com/locate/ybrbi

AVNP2 protects against cognitive impairments induced by C6 glioma by suppressing tumour associated inflammation in rats

Junyang Li^{a,1}, Meicen Liu^{a,1}, Jin Gao^a, Yu Jiang^a, Limin Wu^b, Yuen-Ki Cheong^c, Guogang Ren^c, Zhuo Yang^{a,*}

^a Medical School, State Key Laboratory of Medicinal Chemical Biology, Key Laboratory of Bioactive Materials for Ministry of Education, Nankai University, Tianjin 300071, China

^b Institute of Laser and Optoelectronics, School of Precision Instruments and Optoelectronics Engineering, Tianjin University, Tianjin 300072, China

^c Science and Technology Research Institute, University of Hertfordshire, Hatfield, Herts AL10 9AB, UK

ARTICLE INFO

Keywords:

C6 glioma
AVNP2
Cognitive function
Inflammation

ABSTRACT

Glioblastoma is a kind of malignant tumour and originates from the central nervous system. In the last century, some researchers and clinician have noticed that the psychosocial and neurocognitive functioning of patients with malignant gliomas can be impaired. Many clinical studies have demonstrated that part of patients, adults or children, diagnosed with glioblastoma will suffer from cognitive deficiency during their clinical course, especially in long-term survivors. Many nanoparticles (NPs) can inhibit the biological functions of tumours by modulating tumour-associated inflammation, which provokes angiogenesis and tumour growth. As one of the best antiviral nanoparticles (AVNPs), AVNP2 is the 2nd generation of AVNP2 that have been conjugated to graphite-graphene for improving physiochemical performance and reducing toxicity. AVNP2 inactivates viruses, such as the H1N1 and H5N1 influenza viruses and even the SARS coronavirus, while it inhibits bacteria, such as MRSA and *E. coli*. As antimicrobials, nanoparticles are considered to be one of the vectors for the administration of therapeutic compounds. Yet, little is known about their potential functionalities and toxicities to the neurotoxic effects of cancer. Herein, we explored the functionality of AVNP2 on inhibiting C6 in glioma-bearing rats. The novel object-recognition test and open-field test showed that AVNP2 significantly improved the neurobehaviour affected by C6 glioma. AVNP2 also alleviated the decline of long-term potentiation (LTP) and the decreased density of dendritic spines in the CA1 region induced by C6. Western blot assay and immunofluorescence staining showed that the expressions of synaptic-related proteins (PSD-95 and SYP) were increased, and these findings were in accordance with the results mentioned above. It revealed that the sizes of tumours in C6 glioma-bearing rats were smaller after treatment with AVNP2. The decreased expression of inflammatory factors (IL-1 β , IL-6 and TNF- α) by Western blotting assay and ELISA, angiogenesis protein (VEGF) by Western blotting assay and other related proteins (BDNF, NF- κ B, iNOS and COX-2) by Western blotting assay in peritumour tissue indicated that AVNP2 could control tumour-associated inflammation, thus efficiently ameliorating the local inflammatory condition and, to some extent, inhibiting angiogenesis in C6-bearing rats. In conclusion,

Abbreviations: NPs, nanoparticles; AVNPs, antiviral-nanoparticles; AMNPs, antimicrobial nanoparticles; SARS, severe acute respiratory syndrome; MRSA, methicillin-resistant staphylococcus aureus; LTP, long-term potentiation; PSD-95, postsynaptic density-95; SYP, synaptophysin; IL-1 β , interleukin-1 β ; IL-6, interleukin-6; TNF- α , tumour necrosis factor- α ; ELISA, enzyme linked immunosorbent assay; WB, western blot; VEGF, vascular endothelial growth factor; BDNF, brain derived neurotrophic factor; NF- κ B, nuclear factor kappa-light-chain-enhancer of activated B cells; iNOS, inducible nitric oxide synthase; COX-2, cyclooxygenase-2; GBM, glioblastoma; TAMs, tumour associated macrophages; TME, tumour micro-environment; THz, terahertz; ATR, attenuated total reflection; DMEM, Dulbecco's modified Eagle's medium; PBS, phosphate buffered saline; XPS, X-ray photoelectron spectroscopy; FTIR, Fourier transform infrared spectroscopy; SD, Sprague-Dawley; NS, normal saline; NOFT, novel object recognition test; RI, recognition index; DI, discrimination index; T1, time 1; T2, time 2; OFT, open field test; CA1, cornu ammonis 1; TBS, theta burst stimulation; DPX, distyrene, plasticizer and xylene; BCA, bicinchoninic acid; SDS-PAGE, sodium dodecyl sulfate polyacrylamide gel electrophoresis; PDVF, polyvinylidene fluoride; TBST, tris buffered saline tween; RT, room temperature; DAPI, 4,6-diamidino-2-phenylindole; SEM, standard error of the mean; ANOVA, analysis of variance; fEPSPs, field excitatory postsynaptic potentials; LSD analysis, least significant difference; ECs, endothelial cells; AD, Alzheimer disease

* Corresponding author at: College of Medicine, Nankai University, Tianjin 300071, China.

E-mail addresses: zhuoyang@nankai.edu.cn, hge@ascentgene.com (Z. Yang).

¹ J. Li, and M. Liu equally contributed to this study.

<https://doi.org/10.1016/j.bbi.2020.02.009>

Received 12 November 2019; Received in revised form 24 January 2020; Accepted 20 February 2020

0889-1591/© 2020 The Authors. Published by Elsevier Inc. This is an open access article under the CC BY-NC-ND license (<http://creativecommons.org/licenses/by-nc-nd/4.0/>).

Please cite this article as: Junyang Li, et al., Brain, Behavior, and Immunity, <https://doi.org/10.1016/j.bbi.2020.02.009>

our results suggested that AVNP2 could have an effect on the peri-tumour environment, obviously restraining the growth progress of gliomas, and eventually improving cognitive levels in C6-bearing rats.

1. Introduction

Glioblastoma (GBM), a kind of tumour originating from neural stem cells, glial progenitors and astrocytes in the central nervous system, is the most malignant subtype of glioma (Zong et al., 2012; Ohgaki and Kleihues, 2005). It has attracted the attention of researchers all over the world for its highly aggressive characteristics, high recurrence rate and high mortality (Graus et al., 2013; Tanaka et al., 2013). At present, surgery combined with radiotherapy and chemotherapy is the most common treatment strategy in clinic (Stupp et al., 2017; Okada et al., 2017). However, the tolerance of tumour cells to therapy makes some residual lesions regrow, so the outcomes have not been satisfactory (Stupp et al., 2009). Furthermore, it has been found that cognitive impairment is one of the most important clinical symptoms and complications of craniocerebral disease in both patients and animal models with gliomas (Solanki et al., 2017; Wang et al., 2011; Weitzner and Meyers, 1997; Van Dyk and Ganz, 2019). Cognitive function occupies an essential position in predicting the prognosis of glioma patients and may even be the first indicator of tumour recurrence after treatment (Crossen et al., 1994; Janelsins et al., 2011; Vecht et al., 2017; Jacob et al., 2018). In addition, metabolic disorders and tumour regeneration may have a negative impact on cognitive function (Williams et al., 2015; Quant et al., 2009). The cognitive impairment caused by the side effects of radiotherapy and chemotherapeutic drugs is prone to the whole cerebral hemisphere (Froklage et al., 2014; Hilverda et al., 2010). Thus, it is important to create some new therapies and develop some new drugs to repair patients' cognitive impairment.

The micro-environment of glioma consists of various types of cells, of which microglia and tumour-associated macrophages (TAMs) are two important cells. They aggregate in and around glioma tissue and participate in the proliferation and invasion of tumour cells (Noy and Pollard, 2014; Wu and Watabe, 2017). There exists a positive correlation between the level of inflammatory cytokines inside the tumour micro-environment (TME) and the poor clinical prognosis of patients (Sorensen et al., 2018). Modulating the local inflammatory response has become a new strategy for immunotherapy due to its vital role in the development of tumours (Graf et al., 2002; Mineharu et al., 2011). Pro-inflammatory cytokines, including interleukin-6 (IL)-6, IL-1 β and tumour necrosis factor- α (TNF)- α that promote tumour proliferation and migration and NF- κ B pathway play important roles in this process (Mostofa et al., 2017; McFarland et al., 2013; Myung et al., 2010). Therefore, drugs and related therapies devoted to modulating peri-tumour inflammation in the treatment of glioblastoma have massive potential both now and in the future.

Some metallic nanoparticles (NPs) and their intermetallics can form graphite-graphene conjugates to produce strong antiviral/antimicrobial abilities and they are considered to be antiviral and antimicrobial nanoparticles (AVNPs/AMNPs) (Cheong et al., 2017). These AVNPs/AMNPs offer promising biomedical applications, including as antimicrobial agents in the environment (e.g. inactivating the H1N1 and H5N1 influenza viruses and the SARS coronavirus) or as vectors for the administration of therapeutic compounds or for the delivery of specific drug (Ren, 2010, 2013). Yet, little is known about the potential and wider spectrum of neuronal cell function, neurotoxic effects to cells or specifically to neuronal cancer cells (Yang et al., 2010).

It has been proved that AMNPs and AVNPs, such as Ag(Ag⁺), Cu (Cu²⁺) and Zn(Zn²⁺), have been developed with proven efficacy (99.999%) against both Gram-positive (G⁺) and Gram-negative (G⁻) bacteria (Cheong et al., 2017; Ren et al., 2009; Bankier et al., 2018), which is similar or close to antibiotic properties *in-vitro* (Wan et al.,

2016). The nano-intermetallics (i.e., AVNP2) can especially effectively inactivate bacteria and inhibit bacterial biofilm formation through ionic releases (0.1–5 ppm of [Cu²⁺-[Ag⁺]]) enhanced by their surface charge (Zeta potential (< -40 mv (Nan et al., 2016; Nan et al., 2015; Ren, 2015, 2016) and surface free energy (> 70 mJ/m²) (Nan et al., 2015)

Terahertz (THz) radiation (He et al., 2018) is useful for a number of scientific and industrial applications, such as molecular spectroscopy, high data-rate communication, and material studies. In particular, terahertz (THz) imaging as one of the candidate technologies for medical imaging has attracted great attention in recent years due to its properties of fingerprint spectrum, safety, and water sensitivity. The research on THz biological imaging has been used in various medical fields, such as dermatology and oncology (Sim et al., 2013; Woodward et al., 2003; Reid et al., 2011; Park et al., 2017). In the field of neurosurgery, investigations of gliomas using THz spectrum and THz reflection imaging have also been reported for post-processed, fresh *ex vivo* and *in vivo* brain tissues (Park et al., 2017; Oh et al., 2014; Meng et al., 2014; Wu et al., 2019). However, reflection imaging is always affected by diffusive reflections because of the uneven surface of the sample. Attenuated total reflection (ATR) can provide information on the interaction between the sample and evanescent waves traveling along a prism's surface. Thus, ATR imaging can obtain the precise absorption information of the tissue without inevitable noises.

In this paper, we focused on exploring THz ATR imaging to discriminate tumour from normal brain tissue. We demonstrated that tumours in freshly excised whole brain tissue could be clearly differentiated from normal brain tissue using this imaging system.

Antiviral nanoparticle 2(AVNP2) is an antiviral nanomaterial, which has been shown to kill the SARS virus *in vitro* (Ren et al., 2013). With increasing studies on the application of nanomaterials in the immunotherapy of tumours, a great deal of reports have been published suggesting that nanomaterials can inhibit TAMs to detain the release of related inflammatory factors to achieve the inhibition of tumour growth (Ovais et al., 2019; Gong et al., 2019; Reichel et al., 2019). Thus, we hypothesised that AVNP2 can inhibit the proliferation of C6 glioma cells in rats and can in turn further improve the cognitive impairment of C6 model rats in terms of tumour cell reduction.

As a result, in this study, we proved that AVNP2 could rescue the cognitive impairment of C6 glioma-bearing rats by restraining peri-tumour inflammation and impede the growth of tumour cells.

2. Materials and methods

2.1. Cell culture

C6 glioma cells (ATCC, USA) were cultured in Dulbecco's modified Eagle's medium (DMEM; Gibco BRL, USA) with antibiotics and 10% foetal calf serum. Culture media was placed in the environment with a humidified atmosphere of 5% carbon dioxide (CO₂)/98% air, and the temperature was maintained at 37 °C. When the cultures became 80%–90% confluent, they were washed by phosphate-buffered saline (PBS). Afterwards, C6 cells were suspended in DMEM at the concentration of 1.0 × 10⁶ cells per 100 μ l in a tube for brain tumour xenograft.

2.2. Materials

The AVNP2 used in this study was acquired from the Antimicrobials@UH team, representing the AVNP Consortium in the UK, Institute of Science and Technology, University of Hertfordshire, Hatfield, UK. The transmission electron microscopy (TEM) of the

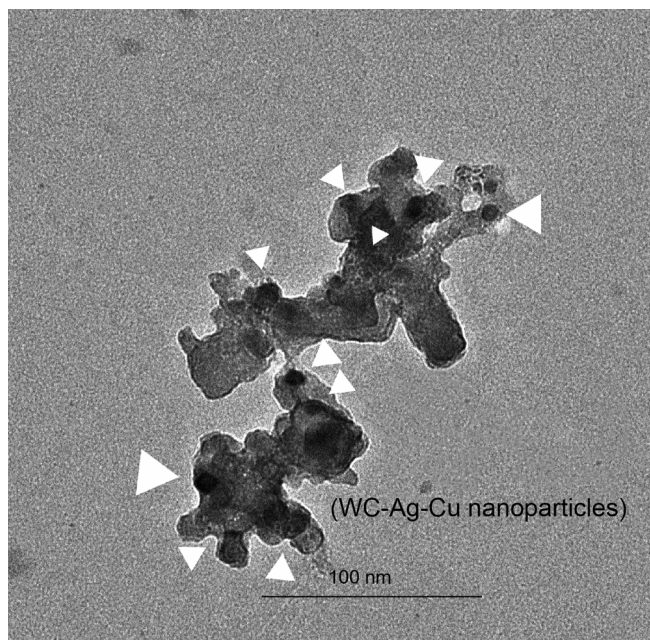


Fig. 1. The TEM (transmission electron microscope) of nanoparticles: AVNP2. The TEM was used to examine internal and amorphous structures of the AVNP2 particles. As arrows indicated, the effective nanoparticles of W-Ag-Cu intermetallics and other trace elements are shown as darkened spots with the sample image, and they are wrapped with elemental carbon compounded sp² graphene/graphite bonding structures. The metal intermetallics were distributed uniformly within the carbon nanostructured particles as white arrows indicated their location and nano-sizes with the particle demine. The differentiation and average sizes were measured in between 10 and 30 nm, which proved the particles containing multiple elemental conjugations.

structure of AVNP2 is shown in Fig. 1. As indicated in the TEM, the paralleled chemical analysis that measuring the AVNP2 nanoparticles was carried out by research groups elsewhere using multiple analytical instruments including XPS, FTIR, Raman Spectroscopy, Solid State Carbon-13 Nuclear Magnetic Resonance spectroscopy, Powder X-ray Diffraction and X-Ray Photoelectron Spectroscopy (Ren et al., 2009; Cheong et al., 2017). AVNP2 was suspended in saline solution (0.9% NaCl) at a concentration of 1 mg/ml, and the suspension was sonicated for 10 min before injection into the brain.

2.3. Animals

Specific-pathogen free adult male Sprague-Dawley (SD) rats, weighing 250–300 g, were purchased from the Experimental Animal Centre at the Chinese Academy of Medical Science. Before the experiments, they were kept in an animal house allocated at the Medical School of Nankai University. They were receiving common feed and water (5 rats in each cage) at a room temperature (RT) of 20 ± 2 °C and 12 h light/dark cycle per day based on the regulations and standards required. All experiments conformed to the protocols ratified by the Committee for Animal Care at Nankai University and corresponded to the practices outlined in the NIH Guideline for the Care and Use of Laboratory Animals. Rats were acclimated for about 1 week before the experiments.

Rats were randomly divided into four groups: Sham group ($n = 6$), Sham + AVNP2 group ($n = 6$), C6 group ($n = 6$) and C6 + AVNP2 group ($n = 6$).

2.4. C6 model surgery and treatment

The rats were deprived of food and water for 12 h before surgery. After being anesthetized with pentobarbital sodium (50 mg/kg,

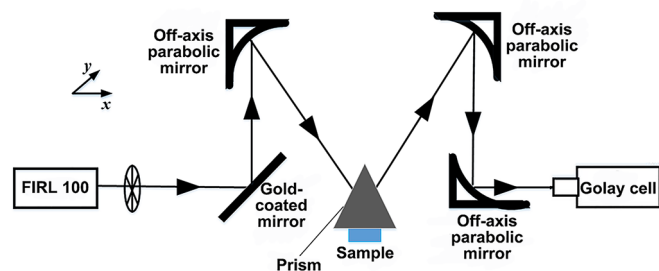


Fig. 2. Schematic of THz attenuated total reflection imaging setup. This method with an isosceles triangle shaped silicon prism can provide information on the interaction between the sample and evanescent wave traveling along a prism surface. The surface information of the sample in close contact with a prism can be acquired by two-dimensionally scanning of this prism moving in the x-y plane.

intraperitoneal injection), the rat's scalp was incised along the top of the head about 1–2 cm long to expose the top of the skull. A small hole with diameter of 1 mm was drilled in the right 3 mm and posterior 0.5 mm of the bregma. C6 cells ($1 \times 10^6/10 \mu\text{l}$) were injected into the rat's cranial cavity vertically at the depth of 5 mm from the dura mater with a speed of 1 $\mu\text{l}/\text{min}$. The needle was retained for 10 min before withdrawal. Then the skin was sutured. Rats of the Sham + AVNP2 and C6 + AVNP2 groups were given AVNP2 the day after the surgery. The AVNP2 suspension was injected into the body of rats at the dose of 3 mg/kg through the vena caudalis once a day for a week. Rats of the Sham and C6 groups were given the equal amounts of normal saline (NS) at the same time. On day 8 post-implantation, calliper measurements were used to assess tumour size.

2.5. Weight recording and tumour specimens

From the day of modelling surgery, the weights of each group were recorded at 10 a.m. daily. After the electrophysiological experiment, the rats were killed by neck rupture, the skull was opened quickly and the whole brain was removed. The transplanted tumours were removed, and the volumes of the tumours were measured.

2.6. Terahertz (THz) radiation

The basic structure diagram of the THz imaging system is shown in Fig. 2. An optically pumped THz gas laser (FIRL100, Edinburgh Instruments Ltd.) was used. The maximum THz output power of this gas laser can reach up to 150 mW at 2.52 THz. Gold-coated flat mirrors and three off-axis parabolic reflectors were used to reflect and focus the THz waves on samples and guide reflected waves to the detector. The focal length of the parabolic reflector used was 2 in. and the F-number was 1. Golay cells (GC-1P, Tydex Ltd.) were used as the detectors and the THz wave was modulated as a sinusoidal signal using the chopper operating at 50 Hz. The spatial resolution of this imaging system was $400 \times 450 \mu\text{m}$ at 2.52 THz. The two dimensional (2D) movable sample stages were used for THz images, and the scanning speed was 10 pixels/s. The scanning step was set as 200 μm , and the temperature was kept constant during all experiments.

2.7. Novel object recognition test (NORT)

The experiment was divided into two stages: the training stage and the testing stage. In the training stage, the two same objects (A and B) were placed in the 60 cm \times 60 cm \times 40 cm test box on the diagonal line. The distance from the rats to the two objects was equal at the beginning of the test. We recorded the exploratory behaviour of objects A and B in over 10 min period. After 1 h, the test phase was carried out. In this phase, object B was changed into object C, which was totally

different from objects A and B. The exploratory time lasted for 10 min and results were recorded. The time spent exploring a familiar object (time 1, T1) and time spent exploring a novel object (time 2, T2) were recorded. The recognition index (RI; $RI = T2/(T1 + T2)$) and discrimination index (DI; $DI = (T2 - T1)/(T2 + T1)$) (d'Isa et al., 2014) were used to evaluate the cognitive level of rats. Both of them showed a degree of preference of rats for new objects, while the former could take into account the individual preferences of rats in the training stage (d'Isa et al., 2014).

Besides, the distance travelled, total object exploration time and velocity of movement were also calculated to validate the test results. After each experiment, the inside of the reaction chamber was cleaned up with 75% alcohol.

2.8. Open field test (OFT)

The bottom surface of the open field reaction chamber (60 cm × 60 cm × 40 cm) was divided into 4 × 4 grids. The four grids in the centre were defined as the central grids, and the 12 grids around it were defined as the surrounding grids. The experiments were carried out at 9:00 a.m. and the experimental site maintained a weak light source. The rats were placed in the centre of the bottom of the reaction chamber for 10 min. Meanwhile, the camera above the box recorded the activity of the rats. The chamber was cleaned with 75% alcohol after each experiment. The recording indices included the residence time of animals in the central grids, and the mean arean speed was calculated to validate the test results.

2.9. Electrophysiological experiment

The hippocampal synaptic plasticity between the Schaffer collaterals and CA1 pyramidal neurons of each rat was measured after the OFT. The rat was anesthetized with 30% urethane (4 ml/kg) by intraperitoneal (i.p.) injection and was placed on the stereotaxic frames (SR-6 N; Narishige, Japan). The rat's scalp was incised, and a small hole in the left side of the skull was drilled. The recording electrode was inserted into the rat's hippocampal CA1 region (3.5 mm posterior to the bregma, 2.5 mm lateral to the midline, and 1.5–2.5 mm ventral below the dura), and the bipolar stimulating electrode was inserted into the rat's hippocampal Schaffer collaterals region (4.2 mm posterior to the bregma, 3.5 mm lateral to the midline, and 2–3.5 mm ventral below the dura). The optimal stimulating intensity (range 0.3–0.5 mA) evoking a response of 50% of its maximum amplitude was delivered at single-pulse stimulation (stimulus pulse 0.2 ms at 0.03 Hz) to record a 20 min baseline. After recording the baseline, a theta burst stimulation (TBS), which was evoked by a Master 8 pulse stimulator (A.M.P.I., Jerusalem, Israel) consisting of 30 trains of 12 pulses (200 Hz) at 5 Hz, was applied to simulate long-term potentiation (LTP). Then, the single-pulse stimulation was resumed at 60 s intervals for 1 h at the baseline intensity. The initial data collections were analysed in Clampfit 10.0 (HEKA, Germany).

2.10. Golgi-cox staining

The hippocampus was placed in Golgi-cox solution. The Golgi-cox solution was renewed 3 days at a time. Then, the tissues were sliced into 150 μm sections. The slices were immersed in the following order: 6% Na₂CO₃ 20 min, distilled water 1 ~ 2 s, 70% ethanol 10 min, 90% ethanol 15 min, anhydrous ethanol 20 min and xylene 20 min. Finally, the slices were fixed on the slide with DPX and covered with glass. The sections were observed by positive fluorescence microscopy. Dendritic spine density was estimated by drawing segments about 20 μm long under a high power mirror (×1000) and counting the spine numbers (Sholl et al., 1953). The dendritic spine density of pyramidal cells with apical dendrites in the CA1 region was calculated. Then, we classified the dendritic spines into four types based on their morphology:

mushroom (the head of a spine larger than 0.6 μm in diameter), stubby (short spine with no head), thin (long spine with a small head, no larger than 0.6 μm in diameter) and filopodia (long with no head) (Sorra and Harris, 2000).

2.11. Western blot analysis

Meanwhile, the left hippocampal tissues of the rats in each group, the peri-tumour tissues of the rats in the C6 group and C6 + AVNP2 group and the corresponding tissues in the same part of rats in the Sham group and Sham + AVNP2 group were taken out. The tissues were cracked and crushed on ice with pyrolysis solution (Beyotime Biotechnology, Haimen, China). The treated tissues were centrifuged at a speed of 12,000 rpm for 30 min at 4 °C and the precipitate was removed. The protein contents of these tissues were determined by the BCA method (Beyotime Biotechnology, Haimen, China). In the remaining supernatant, 4× loading buffer was added according to the remaining supernatant at the ratio of 1:3, and the liquid was boiled for 15 min at 100 °C.

Equivalent amounts of protein (20 μg) from every group (n = 3) were separated by SDS-PAGE gel electrophoresis. Afterwards, these proteins were transferred to polyvinylidene fluoride (PVDF) membranes (Millipore, USA). Then, the PVDF membranes were blocked by 5% skimmed milk powder for 1 h at RT. Subsequently, the membranes were incubated with primary antibodies (anti-β-actin, 1:5000, Abcam; anti-PSD-95, 1:2000, Abcam; anti-SYP, 1:2000, Abcam, anti-NF-κB p65, 1:500 Abcam; anti-VEGF, 1:2000, Abcam; anti-BDNF, 1:2000, Abcam; and anti-IL-1β, 1:500; anti-IL-6, 1:500; anti-TNF-α 1:500; anti-inducible nitric oxide synthase (iNOS), 1:200; and anti-COX-2, 1:200 – all purchased from Santa Cruz Biotechnology) for a night at 4 °C. After being incubated by the primary antibodies, the membranes were washed with TBST and incubated with the secondary antibodies (1:5000) for 1 h at RT. The membrane was cleaned again with TBST. The protein bands were detected by chemiluminescent HRP substrate (Tanon Technology Co., Ltd, Tanon 5500). Image J software (NIH, Bethesda, MD) was applied to determine the quantification of the protein bands.

2.12. Enzyme-linked immunosorbent assay (ELISA)

The brain tissue around the glioma site and prefrontal lobe were orderly collected and washed. Then, the homogenate was centrifuged at 6000 × g at 4 °C for 5 min. The supernatant was collected and prepared for a succeeding assay. The levels of IL-6, IL-1β, and TNF-α in the supernatants were measured following the manufacturer's instructions by using the rat Cloud-Clone Crop. ELISA kit (Houston, USA; IL-1β, SEA563Ra, 96 T; IL-6, SEA079Ra, 96 T; TNF-α, SEA133Ra, 96 T).

2.13. Immunofluorescence staining

Immunofluorescence staining was done as previously described (Zhang et al., 2017). Rats were perfused with 0.1 mol/l PBS (pH = 7.4) to remove the blood. Then, the brain was cut into 8 μm thick slices on the coronary plane. Slices were permeabilized in 0.3% Triton X for 5 min. Then, they were washed with PBS for 5 min twice. Afterwards, the slices were blocked in 10% goat serum for 2 h at RT and were incubated with primary antibodies (PSD95: 1:100, Abcam Ltd. USA; SYP: 1:100, Abcam Ltd. USA) overnight at 4 °C. On the second day, slices were incubated with secondary antibodies (Abcam 594-conjugated, USA) for 1 h at RT. Before microscopic examination, the nuclei were stained with 4,6-diamidino-2-phenylindole (DAPI) for 5 min. Fluorescent signals were notarized using a laser scanning confocal microscope (Olympus F1000, Japan). The number of immunofluorescence labelled PSD-95-positive and SYP-positive cell bodies were quantified in the cerebral cortex. There were four rats for each group, with four slices of each rat. All immunofluorescence staining images were quantified by ImageJ software.

2.14. Data and statistical analysis

In this study, all data were shown as mean \pm standard error of the mean (SEM). Data from the behavioural tests, LTP recordings, Western blot assay, ELISA assay, immunofluorescence staining and Golgi-cox staining were analysed by two-way ANOVA with the post *hoc* test behind. Data from the volume of tumours were analysed by *t*-test. Statistical differences were considered when $P < 0.05$. The statistical analyses were all calculated by using SPSS (version 16.0) software.

3. Results

3.1. Effects of AVNP2 on the weight of rats and the size of tumours

As shown in Fig. 3a, rats in all groups gained weight steadily within eight days of the modelling, and there was no statistically significant difference among the four groups (Fig. 3a, $F = 0.2217$, $P = 0.9999 > 0.05$). The growth of the tumour in the brain is the main reason for poor outcomes and deaths in both humans and experimental animals (Ohgaki and Kleihues, 2005). To figure out the effects of AVNP2 on the growth of C6-glioma *in vivo*; we separated the tumour after the rats were sacrificed and measured the size of the tumour using callipers. As shown in Fig. 3b and c, six glioma specimens from the C6 group and C6 + AVNP2 group are shown and the glioma size of the C6 + AVNP2 group is clearly suppressed as compared with that of the C6 group (Fig. 3b and c, $P = 0.0276 < 0.05$).

3.2. Thz ATR imaging to discriminate tumour region

To compare the normal and glioma brain tissue quantitatively, the reflectivity divided by THz was used to reflect the intensity signal from without and within the sample. Visual images, THz images, and reflectivity for fresh brain tissue with and without tumours are shown in Fig. 4. Three images of brain tissue were obtained without tumour (a) and with tumours (b and c). Each pixel was described by reflectivity. The tumour region appeared darker in the visible images, which was marked by dashed lines in the visual images. It was clearly seen that the THz images for the normal brain tissue looked uniform and THz images of glioma tissue showed obvious differences in the tumour region as compared with the normal tissue, as shown in the red regions in the THz images. The detailed profile of the reflectivity values along the

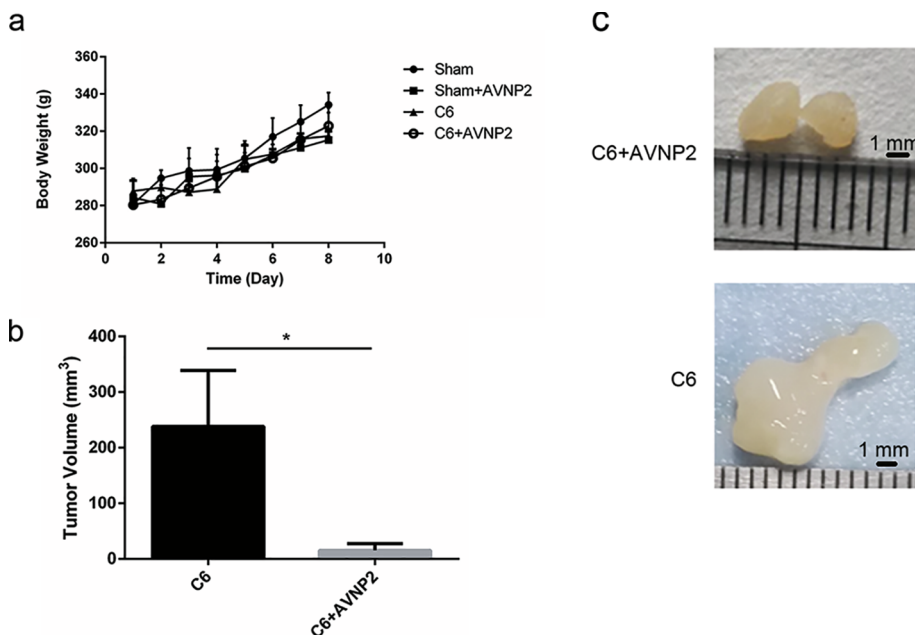


Fig. 3. Effects of AVNP2 administration on rats' body weight gain in sham group, sham + AVNP2 group, C6 group and C6 + AVNP2 group every day. Rats' Body Weight was measured every day at noon for eight consecutive days. It showed no statistic difference among four groups, $P > 0.05$. Effects of AVNP2 administration on C6 growth *in vivo*. Data are expressed as mean \pm SEM, $n = 6$ per group. Fig. 3b: AVNP2 reduced the size of glioma growth in the rat's model. Fig. 3c: typical photos of tumours in C6 group and C6 + AVNP2 group. Data represented mean \pm SEM, $n = 3$ per group, $*P < 0.05$.

horizontal purple lines of the THz images were as shown in the reflectivity images (Fig. 4). The reflectivity values of the tumour region were lower than 30%, whereas the reflectivity values for the normal tissues were rarely lower than 30%. Considering all the samples, the dynamic range of the reflectivity values for the normal and tumour tissues were $27\% \pm 2\%$ and $32\% \pm 3\%$, respectively.

3.3. Effects of AVNP2 on cognitive ability (NORT) of rats with glioma

The mode pattern is shown in Fig. 5a. In the training stage, the exploration ratio among the groups showed no statistically significant difference (Fig. 5b, $F = 1.107$, $P = 0.3566 > 0.05$). In the testing stage, we calculated the RI (the formula: $RI = T2/(T1 + T2)$). There was a statistically significant difference between the four groups by two-way ANOVA test (Fig. 5c $F = 11.72$, $P = 0.0001 < 0.001$). Then, through multiple comparisons test, we found that there was a statistically significant difference between the Sham group and C6 group (Fig. 5c, $F = 0.3533$, $P = 0.0026 < 0.01$). Specifically, the rats of the C6 group had some defects with memory and learning ability as compared to the Sham group. Moreover, after treatment with AVNP2, the RIs of rats in the C6 + AVNP2 group were obviously increased (Fig. 5c, $F = -0.4475$, $P = 0.0001 < 0.001$). There was no statistically significant difference between the Sham group and Sham + AVNP2 group (Fig. 5c, $F = 0.04924$, $P = 0.5769 > 0.05$), which meant that this drug had no side-effects with regard to the cognitive function of rats. We also calculated the DIs of the four groups. There was a statistically significant difference between the Sham group and C6 group (Fig. 5d, $F = 0.7067$, $P = 0.0026 < 0.01$). Meanwhile, there was no statistically significant difference between the Sham group and Sham + AVNP2 group (Fig. 5d, $F = 0.09849$, $P = 0.5769 > 0.05$), which corresponded to the results for the RIs. The distance travelled and velocity of movement showed no difference among the four groups (Fig. 5e, $F = 1.298$, $P = 0.3026 > 0.05$; Fig. 5g, $F = 1.298$, $P = 0.3026 > 0.05$). There was a statistically significant difference between the Sham group and C6 group in total object exploration time (Fig. 5f, $F = 3.190$, $P = 0.0459 < 0.05$).

3.4. Effects of AVNP2 on exploratory behaviours (OFT) of rats with glioma

The OFT was carried out secondly, in order to remove the influence of activity ability on the cognition results. We measured the arean speed

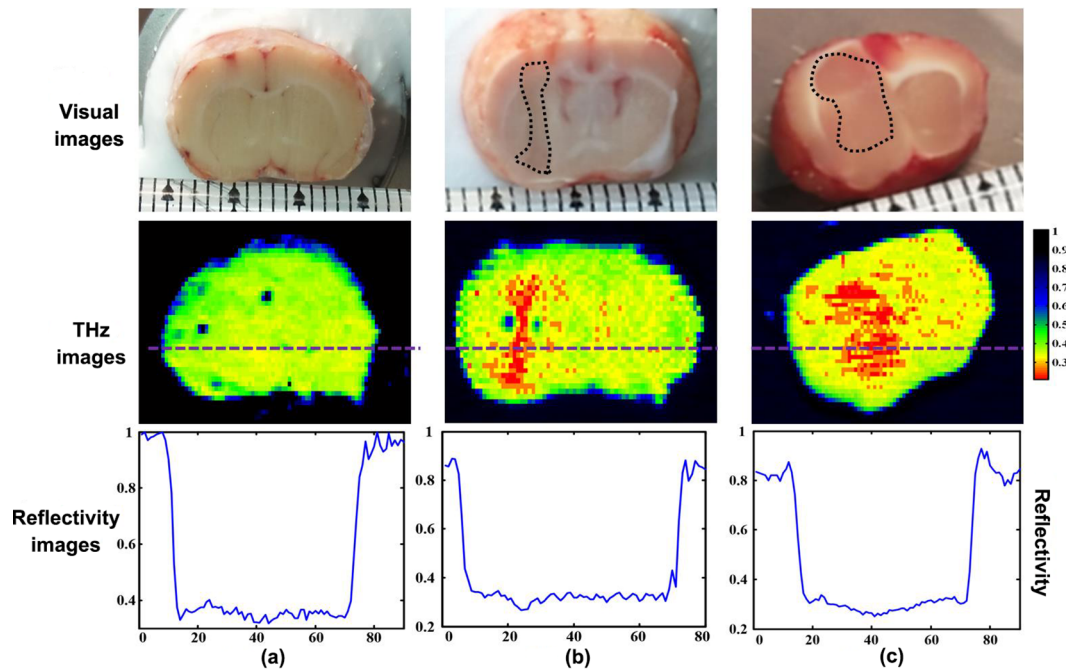


Fig. 4. The results of terahertz (THz) radiation test. Visual imaging, THz imaging and the reflectivity at the horizontal purple line of THz images about freshly excised brain tissues without (a) and with (b, c) tumours. The high absorption regions of THz wave are tumour regions, as the red areas shown in THz images. The value of the reflectivity of the tumour regions was less than 30%, corresponding to the dotted line shown in reflectivity images.

of rats in all groups during the test, and it was found that there was no statistically significant difference among all groups for the OFT (Fig. 6a, $F = 0.1789$, $P = 0.9101 > 0.05$). In this test, there was a statistically significant difference for the time spent in the central compartment among the four groups (Fig. 6b, $F = 3.862$, $P = 0.0249 < 0.05$). Rats of the Sham group stayed longer in the central compartment as compared to those of the C6 group (Fig. 6b, $F = 19.42$, $P = 0.0065 < 0.01$). The performance of C6 model rats treated with AVNP2 was much better than performance of C6 model rats without intervention (Fig. 6b, $F = -18.32$, $P = 0.0296 < 0.05$). There was no statistically significant difference for the time spent in the central compartment between the Sham group and Sham + AVNP2 group (Fig. 6b, $F = 4.317$, $P = 0.4603 > 0.05$).

3.5. Effects of AVNP2 on electrophysiological experiments of rats with glioma

As shown in Fig. 7a, before TBS, the baseline fEPSPs of all four groups were very stable under low-frequency stimulation. After the TBS stimulation, the slopes of the fEPSPs were significantly increased within the following 60 min, except the rats in the C6 group that were lower than the other groups (Fig. 7a). The slopes of the fEPSPs for LTP in the C6 group were apparently decreased as compared to the Sham group (Fig. 7b, $F = 16.5796$, $P < 0.0001$). AVNP2 up-regulated the fEPSPs in the C6 + AVNP2 group (Fig. 7b, $F = 15.7325$, $P < 0.0001$). In addition, there was no statistically significant difference between the Sham group and Sham + AVNP2 group (Fig. 7b, $F = 2.1761$, $P > 0.05$), which meant AVNP2 did not harm synaptic plasticity.

3.6. Effects of AVNP2 on the neuronal dendritic spine density in CA1 region of rats with glioma

Golgi-cox stained CA1 pyramidal neurons are shown in Fig. 8a. The statistical analysis showed that the density of the dendritic spines of the pyramidal neurons in the CA1 region of C6 model rats was obviously less than those of the Sham group (Fig. 8b, $F = 17.40$, $P < 0.0001$). Meanwhile, the density of dendritic spines was significantly increased

in the C6 + AVNP2 group as compared to those of the C6 group (Fig. 8b, $F = -2.272$, $P = 0.005 < 0.01$).

We also compared the frequencies of the four spine types (stubby, mushroom, thin and filopodia) among the four groups. The frequency of stubby spines (mature type) was significantly decreased in the C6 group (29.3%) (Fig. 8c) as compared with the Sham group (42.4%, $P < 0.001$), Sham + AVNP2 group (40.4%, $P < 0.001$) and C6 + AVNP2 group (40.4%, $P < 0.001$) respectively. On the other hand, the frequency of thin spines (immature type) were increased in the C6 group (37.1%) (Fig. 8c) as compared with the Sham group (22.9%, $P < 0.001$), Sham + AVNP2 group (22.8%, $P < 0.001$) and C6 + AVNP2 group (21.3%, $P < 0.001$). These results showed a defect of the mature dendritic spines in the rats of the C6 group and an improvement of the mature dendritic spines in rats of the other groups. All the above suggested that AVNP2 administration prevented the dendritic impairment induced by C6 cells.

3.7. AVNP2 administration increased the expression of synaptic related proteins

PSD-95 and SYP are the two main synaptic-related proteins. As shown in Fig. 9b and d, AVNP2 administration (Sham + AVNP2 group and C6 + AVNP2 group) elevated the expression levels of SYP and PSD-95. (Fig. 9b, $F = 7.908$, $P = 0.0089 < 0.01$; Fig. 9d, $F = 14.81$, $P = 0.0013 < 0.01$). It showed that the expression levels of SYP and PSD-95 were suppressed in the hippocampus of rats in the C6 group as compared with the Sham group (Fig. 9b, $F = 0.2057$, $P = 0.0301 < 0.05$; Fig. 9d, $F = 2.236$, $P = 0.0014 < 0.01$), and the SYP and PSD-95 proteins were relatively elevated in the C6 + AVNP2 group (Fig. 9b, $F = -0.1513$, $P = 0.0023 < 0.01$; Fig. 9d, $F = -1.273$, $P = 0.0393 < 0.05$). There was no statistically significant difference between the Sham group and Sham + AVNP2 group (Fig. 9b, $P = 0.4518 > 0.05$; Fig. 9d, $P = 0.521 > 0.05$).

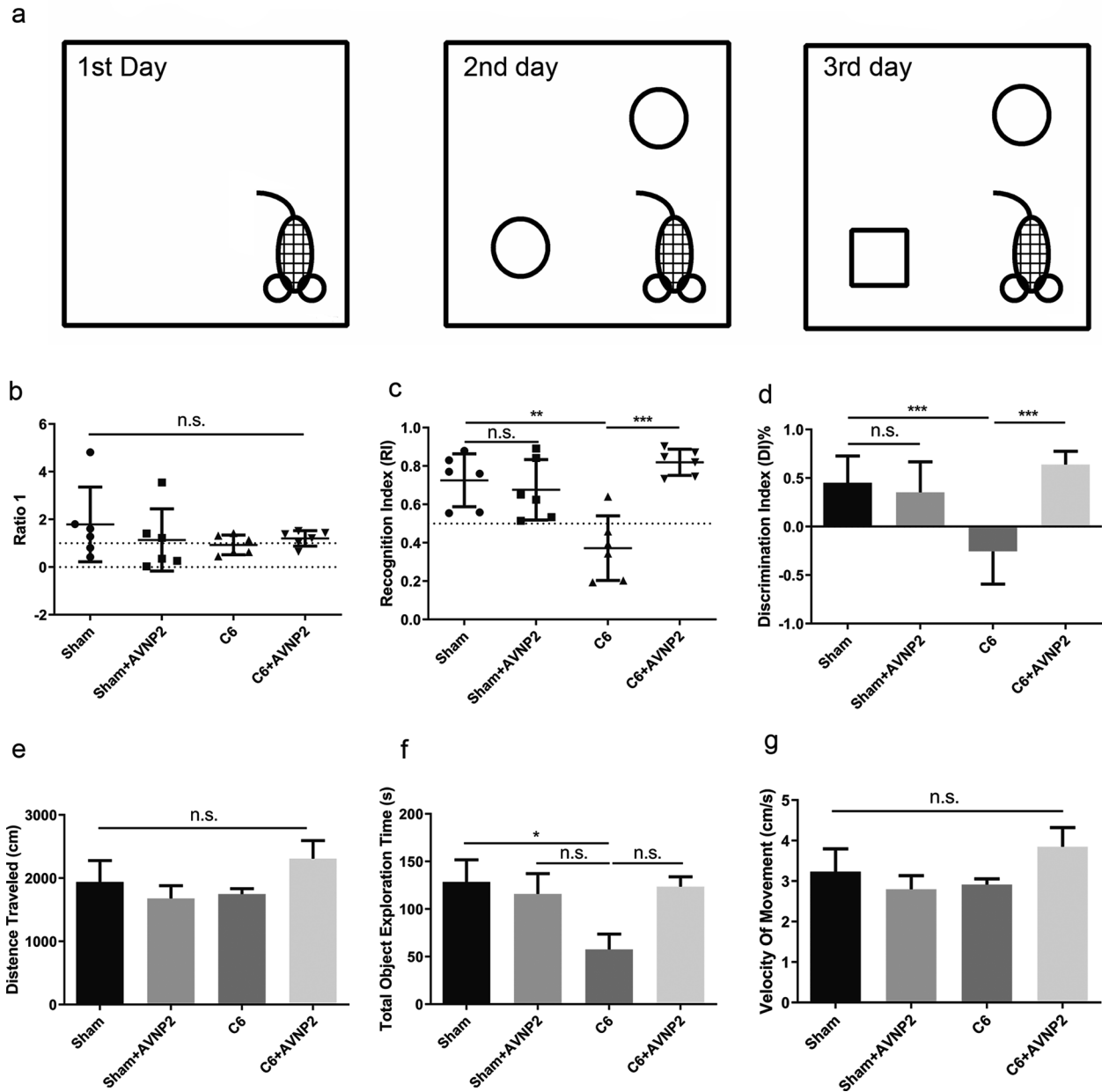


Fig. 5. Effects of AVNP2 administration on novel object recognition test. **a:** the mode pattern of novel object recognition test. **b:** the exploration ratio (Ratio 1) in training stage shows no difference among four groups, $P > 0.05$. **c:** recognition index (RI) in testing stage showed that there exists statistic difference between sham group and C6 group, $**P < 0.01$; C6 group and C6 + AVNP2 group, $**P < 0.01$; the sham group compared to C6 + AVNP2 group, $***P < 0.001$; the sham group compared to C6 + AVNP2 group, $P > 0.05$. **d:** the graph shows the discrimination indexes (DI), the sham group compared to C6 group, $***P < 0.001$; the sham group compared to C6 + AVNP2 group, $***P < 0.001$; the sham group compared to C6 + AVNP2 group, $P > 0.05$. **e:** the graph shows no difference among four groups in distance traveled, $P > 0.05$. **f:** the Total Object Exploration Time results show the statistic difference between sham group and C6 group, $*P < 0.05$; no difference among other groups, $P > 0.05$. **g:** the graph shows no difference among four groups in Velocity Of Movement, $P > 0.05$. Data of Fig. b, c, d, e, f, g represent mean \pm SEM, $n = 6$ per group.

3.8. AVNP2 administration modulated the inflammation in brains of C6-bearing rats

In order to detect whether inflammation played a crucial role in the deficiency of the cognitive status of the rats, we tested the expression of iNOS (130 kDa) and COX-2 (68 kDa). As shown in Fig. 9e and f, COX-2 and iNOS were increased in the peri-tumour tissue of rats in the C6 group as compared to those of the Sham group (Fig. 9e, $F = -1856$, $P < 0.0001$; Fig. 9f, $F = -327.3$, $P < 0.0001$) and the levels of COX-2 and iNOS were reduced in the C6 + AVNP2 group (Fig. 9e, $F = 1014$, $P < 0.0001$; Fig. 9f, $F = 116.8$, $P = 0.0478 < 0.05$), which meant that AVNP2 improved the inflammation in the brain of the rats. As a result, AVNP2 could prevent the injury of neurons in the hippocampus

by reducing the inflammatory proteins and improving the cognitive conditions of rats. There were no statistically significant differences between the Sham group and Sham + AVNP2 group in the expression of COX-2 and iNOS (Fig. 9e, $F = 1.274$, $P = 0.1107 > 0.05$; Fig. 9f, $F = 12.17$, $P = 0.1023 > 0.05$).

3.9. AVNP2 administration suppressed the NF- κ B pathway in rats with glioma

In cerebral peri-tumour tissue, inflammation was accompanied by the activation of the NF- κ B pathway. In order to know whether AVNP2 modulated local inflammation by activating the NF- κ B pathway, we detected the expression of related proteins (Fig. 10a). Western blotting

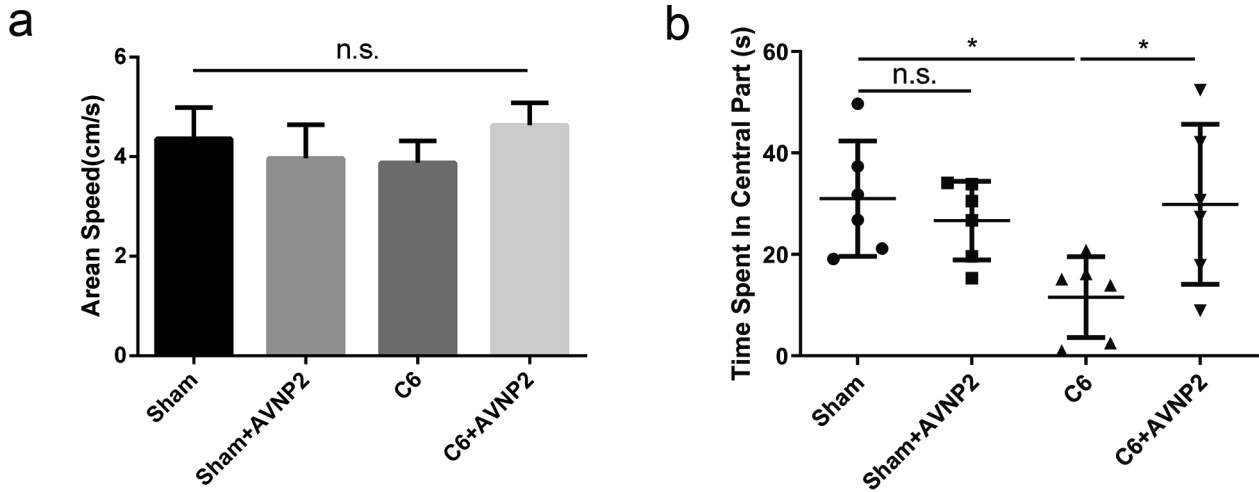


Fig. 6. Effects of AVNP2 administration on open field test. **a:** arean speed was calculated to remove the effect of speed on the results analysis. $P > 0.05$. **b:** Effects of AVNP2 administration on open field test. The graph shows the statistic difference between sham group and C6 group, $*P < 0.05$; C6 group and C6 + AVNP2 group, $*P < 0.05$. Data represent mean \pm SEM, $n = 6$ per group.

results showed that the level of phosphorylated NF- κ B p65 was apparently different among the four groups (Fig. 10b, $F = 15.54$, $P = 0.0011 < 0.01$). The LSD analysis showed that the level of phosphorylated NF- κ B p65 was up-regulated in the C6 group as compared with the Sham group (Fig. 10b, $F = 8.177$, $P = 0.0027 < 0.01$), while this level was down-regulated in the C6 + AVNP2 group (Fig. 10b, $F = 4.175$, $P = 0.0026 < 0.01$). There was no statistically significant difference between the Sham group and Sham + AVNP2 group (Fig. 10b, $F = 1.151$, $P = 0.0950 > 0.05$). Besides, one-way ANOVA analysis showed that there was an apparent difference in the levels of IL-1 β , IL-6, TNF- α and BDNF between the four groups (Fig. 10c, $F = 7.631$, $P = 0.0099 < 0.01$; Fig. 10d, $F = 9.894$, $P = 0.0046 < 0.01$; Fig. 10e, $F = 16.07$, $P = 0.0009 < 0.001$;

Fig. 10f, $F = 7.139$, $P = 0.0119 < 0.05$). AVNP2 administration decreased the level of neuro-inflammation in peri-tumour tissue in C6 + AVNP2 group compared to that of C6 group (Fig. 10c, $F = 36.14$, $P = 0.0022 < 0.01$. Fig. 10d, $F = 59.99$, $P = 0.0080 < 0.01$. Fig. 10e, $F = 55.59$, $P = 0.0073 < 0.01$). AVNP2 administration increased the level of BDNF in the C6 + AVNP2 group as compared with the C6 group (Fig. 10f, $F = -25.61$, $P = 0.0186 < 0.05$). These results tentatively reminded us that AVNP2 administration may down-regulate the neuro-inflammatory response by suppressing the NF- κ B pathway. Furthermore, it may improve the level of cognition. Moreover, we tested the expression of VEGF (Fig. 10g), which represented the level of angiogenesis in the peri-tumour tissue of the brains of rats. We found that the C6 group had a higher level expression of VEGF as compared to

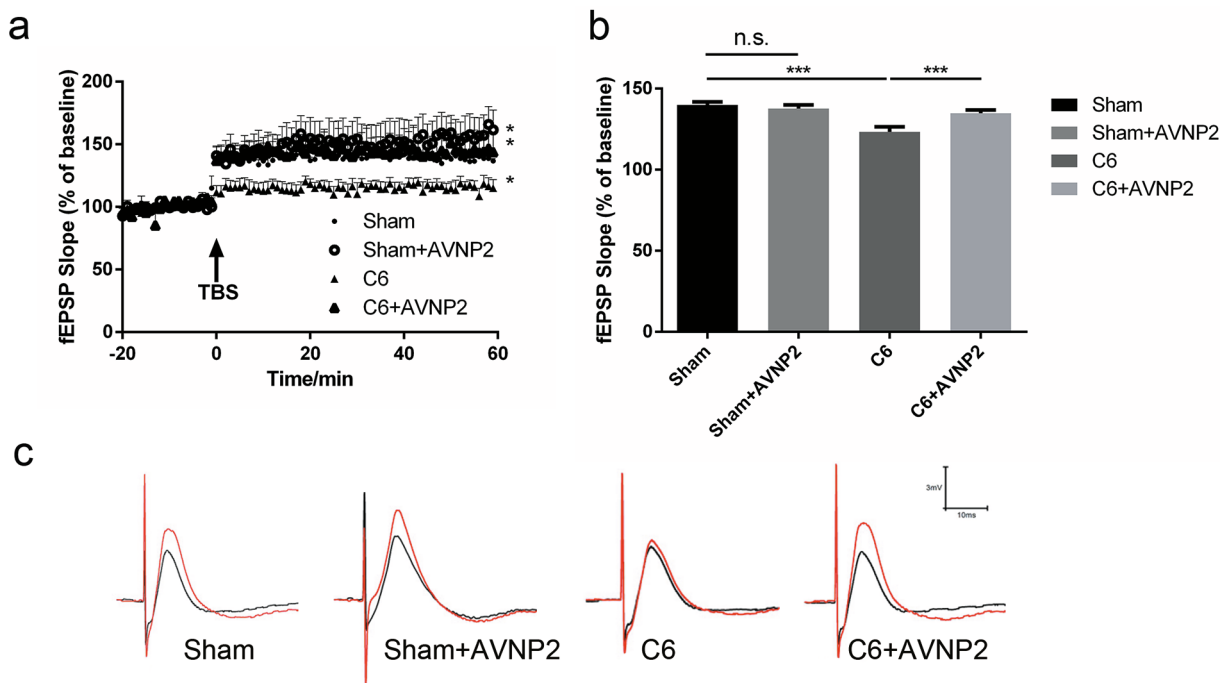


Fig. 7. Effects of AVNP2 administration on LTP. **a:**LTP in the CA3 region was recorded, TBS was used to induce the LTP. **b:** Mean fEPSP slope between 45 and 60 min was regarded as responses, statistic difference was showed between C6 group and sham group/sham + AVNP2 group/C6 + AVNP2 group, $***P < 0.001$. **c:** Effect of AVNP2 on LTP in hippocampal neurons. Data represent mean \pm SEM, $n = 6$ per group.

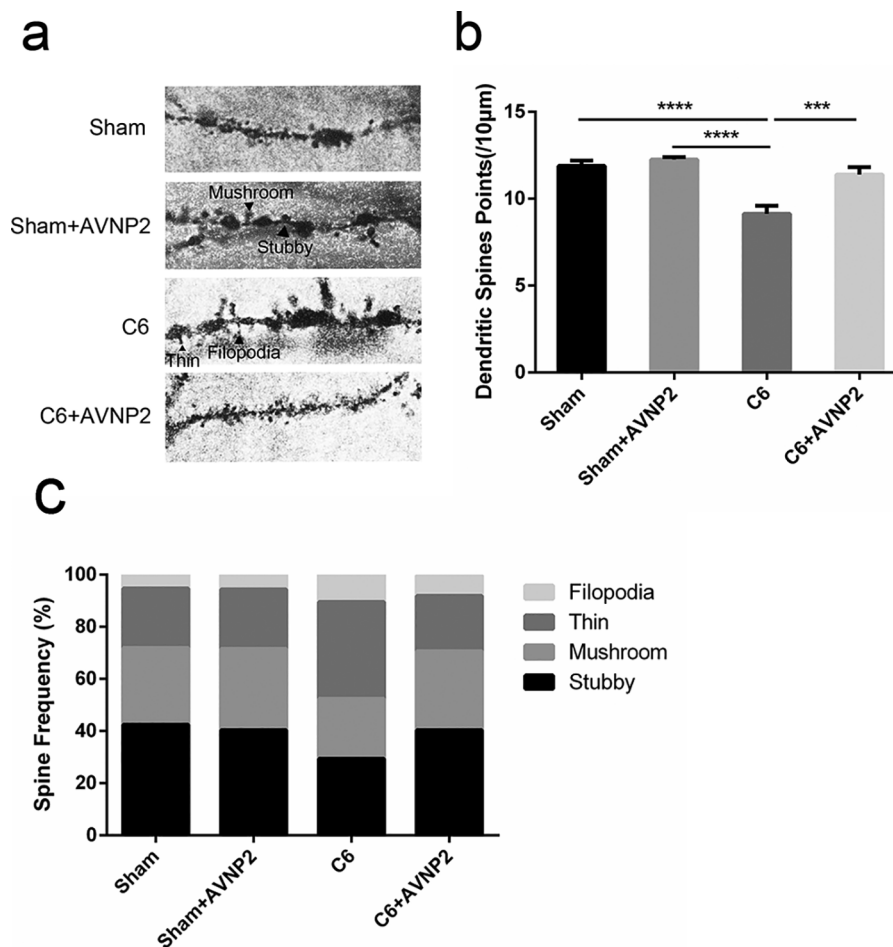


Fig. 8. Effects of AVNP2 administration on hippocampal dendritic morphology. According to morphology, dendritic spines were classified into four types: mushroom, stubby, thin and filopodia. a: The microscope shows the photographs of Golgi stained hippocampal CA1 neuron region. The different types of dendritic spines on the dendrites (indicated by black arrows) are shown. Scalebar, 10 µm. b: The density of dendritic spines of Sham group, Sham + AVNP2 group, C6 group and C6 + AVNP2 group. c: The frequencies of different spine types were calculated. Data represented mean \pm SEM, n = 6 per group. * P < 0.05, ** P < 0.01, *** P < 0.001.

that of the Sham group (Fig. 10h, $F = 6.959$, $P = 0.0084 < 0.01$), while AVNP2 suppressed it in the C6 + AVNP2 group (Fig. 10h, $F = 4.370$, $P = 0.0155 < 0.05$). There was no statistically significant difference between the Sham group and Sham + AVNP2 group (Fig. 10h, $F = -2.864$, $P = 0.1075 > 0.05$).

3.10. AVNP2 administration suppressed the levels of pro-inflammatory cytokines in rats with glioma

Based on the Western blotting results, we detected the levels of IL-1 β , IL-6 and TNF- α by using ELISA in the peri-tumour tissue and prefrontal lobe (Fig. 11a, b, c, d, e and f). The ELISA results showed the levels of IL-1 β , IL-6 and TNF- α were statistically significant different among the four groups (Fig. 11a, b and c; $F = 8.939$, $P = 0.0022 < 0.01$; $F = 306.8$, $P = 0.0001$; $F = 13.55$, $P = 0.0017 < 0.01$, respectively). The LSD analysis showed that the level of IL-1 β , IL-6 and TNF- α were increased in the C6 group as compared with the Sham group in peri-tumour tissue (Fig. 11a, b and c; $F = 41.96$, $P = 0.0019 < 0.01$; $F = 71.87$, $P = 0.0001$; $F = 18.87$, $P = 0.0024 < 0.01$, respectively), while these levels were decreased in the C6 + AVNP2 group (Fig. 11a, b and c; $F = 33.07$, $P = 0.0024 < 0.01$; $F = 64.52$, $P = 0.0001$; $F = 17.16$, $P = 0.0073 < 0.01$, respectively). There was no statistically significant difference between the Sham group and Sham + AVNP2 group (Fig. 11a-c; $F = 1.298$, $P = 0.8355 > 0.05$; $F = 21.46$,

$P = 0.0890 > 0.05$; $F = 1.411$, $P = 0.8295 > 0.05$, respectively). What's more, we also detected these three pro-inflammatory factors in the prefrontal lobe, which plays an important role in emotion regulation but is farther from the glioma as compared to peri-tumour tissue. The ELISA results showed the level of IL-1 β was statistically significant different among the four groups (Fig. 11d, $F = 4.761$, $P = 0.0207 < 0.05$), but there were no statistically significant differences for IL-6 and TNF- α among the four groups (Fig. 11e and f; $F = 2.655$, $P = 0.0754 > 0.05$; $F = 3.120$, $P = 0.0663 > 0.05$, respectively). The LSD analysis showed that the level of IL-1 β was increased in the C6 group as compared with the Sham group in the prefrontal lobe (Fig. 11d, $F = 9.747$, $P = 0.013 < 0.05$) and decreased in the C6 + AVNP2 group in the prefrontal lobe (Fig. 11d, $F = 8.102$, $P = 0.025 < 0.05$).

3.11. The expression of synaptic-related protein changes by immunofluorescence

Immunofluorescence was carried out to validate the neuro-related protein expression changes (Fig. 12c and d). We found a tendency toward a decreasing in the intensities of PSD-95 (Fig. 12a, $F = 2.206$, $P = 0.0234 < 0.05$) and SYP (Fig. 12b, $F = 4.473$, $P = 0.0250 < 0.05$) as compared to the Sham group in the cerebral cortex. However, AVNP2 administration ameliorated the reduced intensities of PSD-95 (Fig. 12a, $F = 1.038$, $P = 0.0459 < 0.05$) and SYP

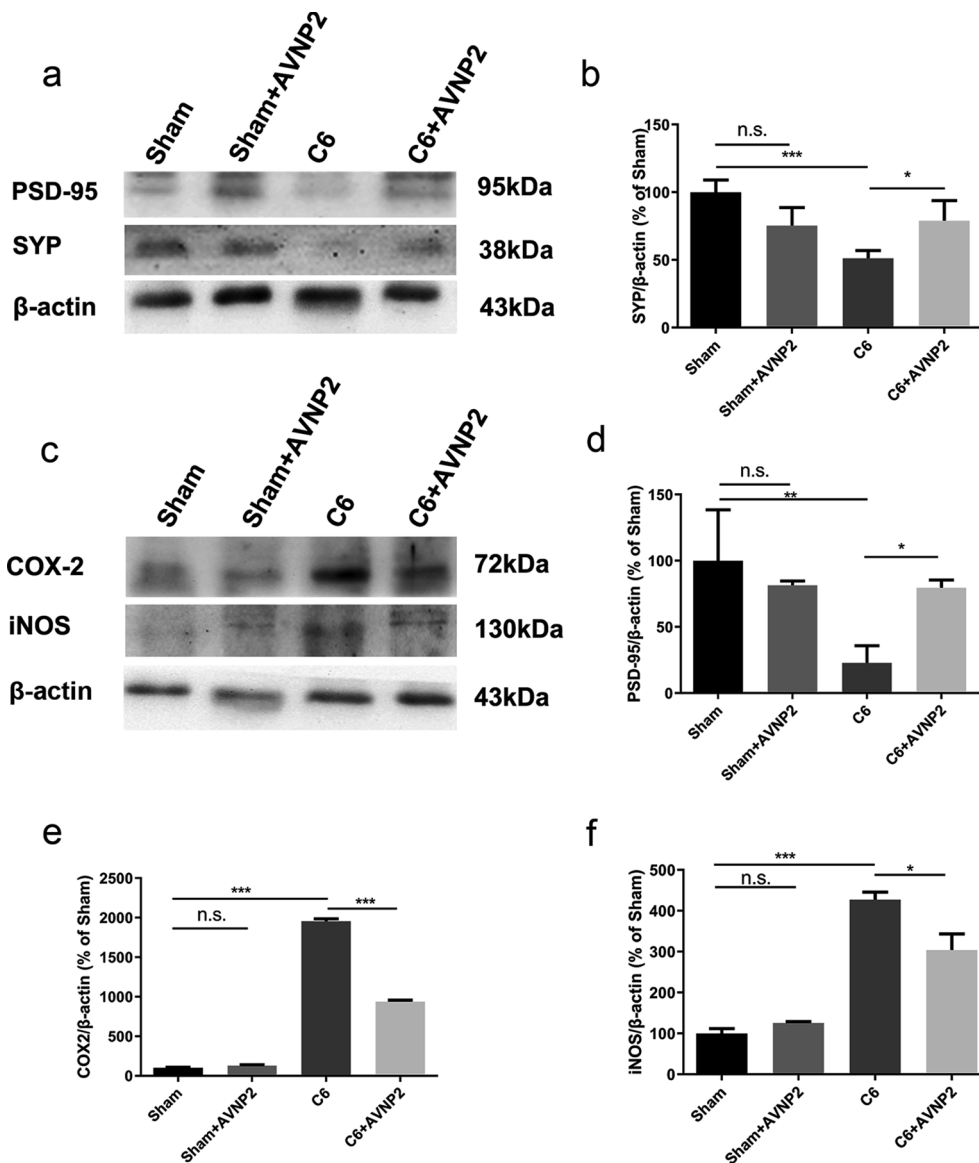


Fig. 9. Effects of AVNP2 administration on synaptic-related and inflammation-related protein. The Western blot assay showed that the levels of PSD-95 from hippocampal tissue of rats of C6 groups were reduced significantly compared with all other groups (Fig. 9b, $*P < 0.05$, $**P < 0.01$). However, protein expression in C6 group treated with AVNP2 had no significant difference with sham group and sham + AVNP2 group (Fig. 9b, $P > 0.05$). The familiar results could be seen in SYP (Fig. 9d). The Western blot assay showed that the levels of COX-2 and iNOS from peritumour tissues of C6 groups were increased significantly compared with all other groups (Fig. 9e, $*P < 0.05$, $**P < 0.001$). However, protein expression in C6 + AVNP2 group had no significant difference with Sham + AVNP2 group (Fig. 9e, $P > 0.05$). The familiar results could be seen in iNOS (Fig. 9f). Data represented mean \pm SEM, $n = 3$ per group, $*P < 0.05$ $**P < 0.001$.

(Fig. 12b, $F = 6.208$, $P = 0.0158$) as compared to the C6 + AVNP2 group. There was no statistically significant difference between the Sham group and Sham + AVNP2 group with regard to the expression of PSD95 and SYP (Fig. 12a and b; $F = 1.131$, $P = 0.0705 > 0.05$; $F = 1.476$, $P = 0.9897 > 0.05$, respectively). These results were correlated with the Western blotting assay results (Fig. 9).

4. Discussion

GBM is one of the most malignant tumours in the central nervous system. An unoptimistic prognosis still exists for even after receiving systematic treatment, with a 5-year survival rate of 5% (Ostrom et al., 2015). The resistance of glioma cells to chemotherapeutic drugs makes it much harder for doctors to control the progression of the tumour. Thus, it is vital for researchers to create new drugs or drug delivery systems to destroy the tumour cells (Saalik et al., 2019). Due to their integrated good physical and chemical properties, NPs have attracted the attention of researchers. In our research, we chose AVNP2 as an anti-inflammatory drug in C6 model rats. AVNP2 proved to inhibit the inflammation induced by viruses *in vitro*. Many studies had proved the gratifying results about tumour growth inhibition by using NPs or NP-delivering systems in animal experiments (Del Sol-Fernandez et al., 2019; Yu et al., 2019; Liang et al., 2018). However, the underlying

mechanisms in NP therapy, especially the change of tumour-associated inflammation inside the tumour environment and peri-tumour tissue, haven't been explained clearly (Ovais et al., 2019). We wanted to investigate whether AVNP2 had a similar effect on gliomas. This time, we found that AVNP2 could not only modulate the tumour associated inflammation but also the levels of inflammation-related proteins such as IL-1 β , IL-6, TNF- α and NF- κ B, which all together play an indispensable role in the formation, growth, infiltration and metastasis of gliomas (Zhu et al., 2017).

Among the inflammatory-related proteins mentioned before, numerous clinical investigations have suggested that their expression in gliomas, peri-glioma tissue and cerebrospinal fluid were significantly higher than that in normal tissue, and the expression level has a positive relationship with the grade of glioma (Shan et al., 2015; Lang et al., 2018; Thompson et al., 2016; Zou et al., 2019). In our study, we tested the level of inflammation-related proteins in peri-tumour tissue using the Western blotting assay and ELISA test, which could be used as a detection marker for treatment. We found the expression in the C6 group was higher than in the normal control group. However, AVNP2 decreased them in the C6 + AVNP2 group and promoted a better TME. A recent study showed that IL-6, IL-1 β and TNF- α could enhance the proliferation and anti-apoptotic ability of glioma stem cells (Wang et al., 2009). Da Silva *et al* used the flavonoid rutin and its aglycone

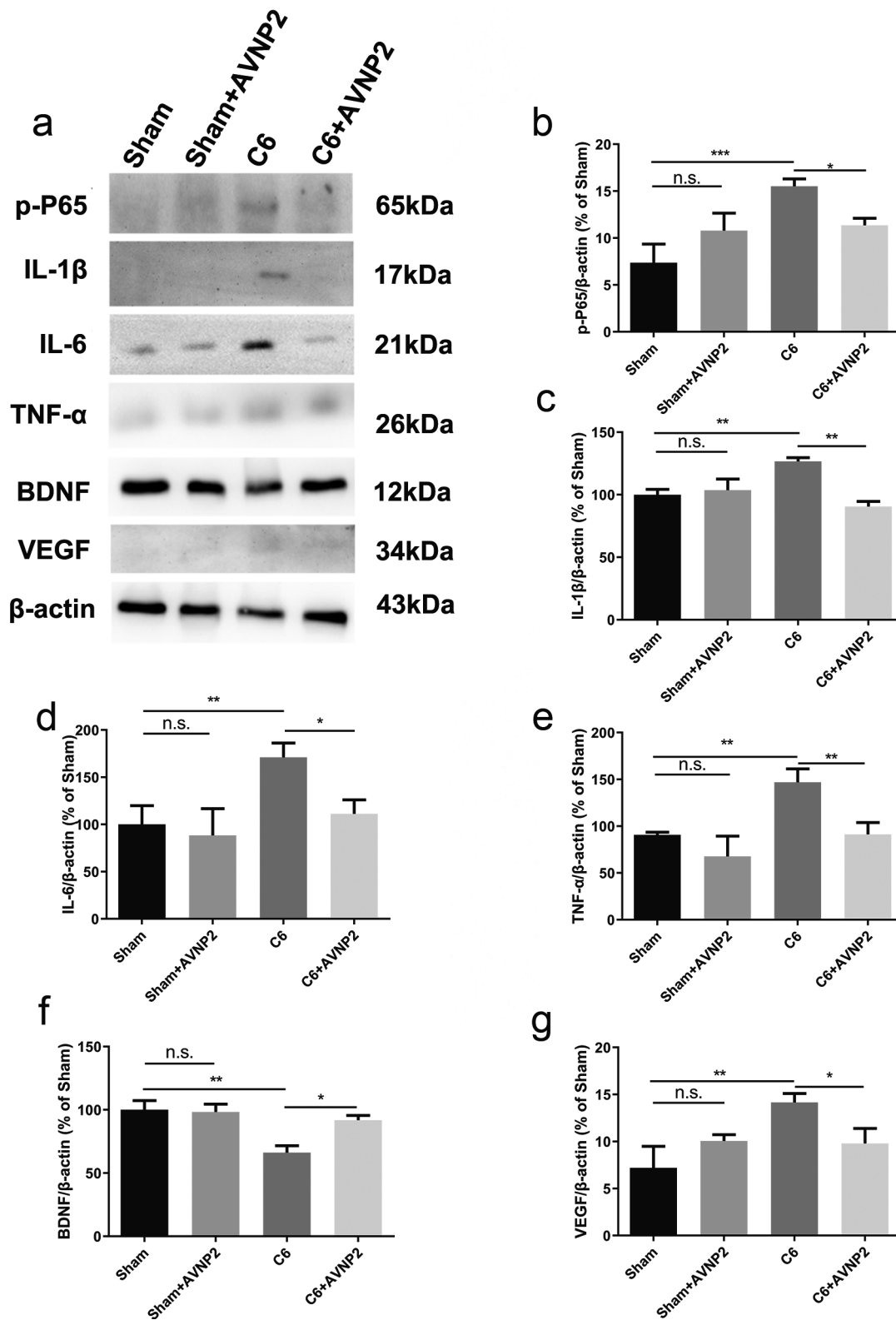


Fig. 10. Effects of AVNP2 administration on NF-κB pathway related protein. The Western blot assay showed that the levels of p-P65 from peri-tumor tissue of rats of C6 groups were increased significantly compared with all other groups (Fig. 10b, $*P < 0.05$, $***P < 0.001$). However, protein expression in Sham group treated with AVNP2 had no significant difference with Sham + AVNP2 group (Fig. 10b, $P > 0.05$). The familiar results could be seen in IL-1β, IL-6, TNF-α (Fig. 10c-e). The level of BDNF was decreased in C6 group compared with other groups (Fig. 10f, $*P < 0.05$, $**P < 0.01$). The results showed that VEGF was evaluated in C6 group (Fig. 10g, $*P < 0.05$, $**P < 0.01$). And there was no difference between sham, sham + AVNP2 and C6 + AVNP2 groups (Fig. 10g, $P > 0.05$). Data represented mean \pm SEM, $n = 3$ per group, $*P < 0.05$, $**P < 0.01$, $***P < 0.001$.

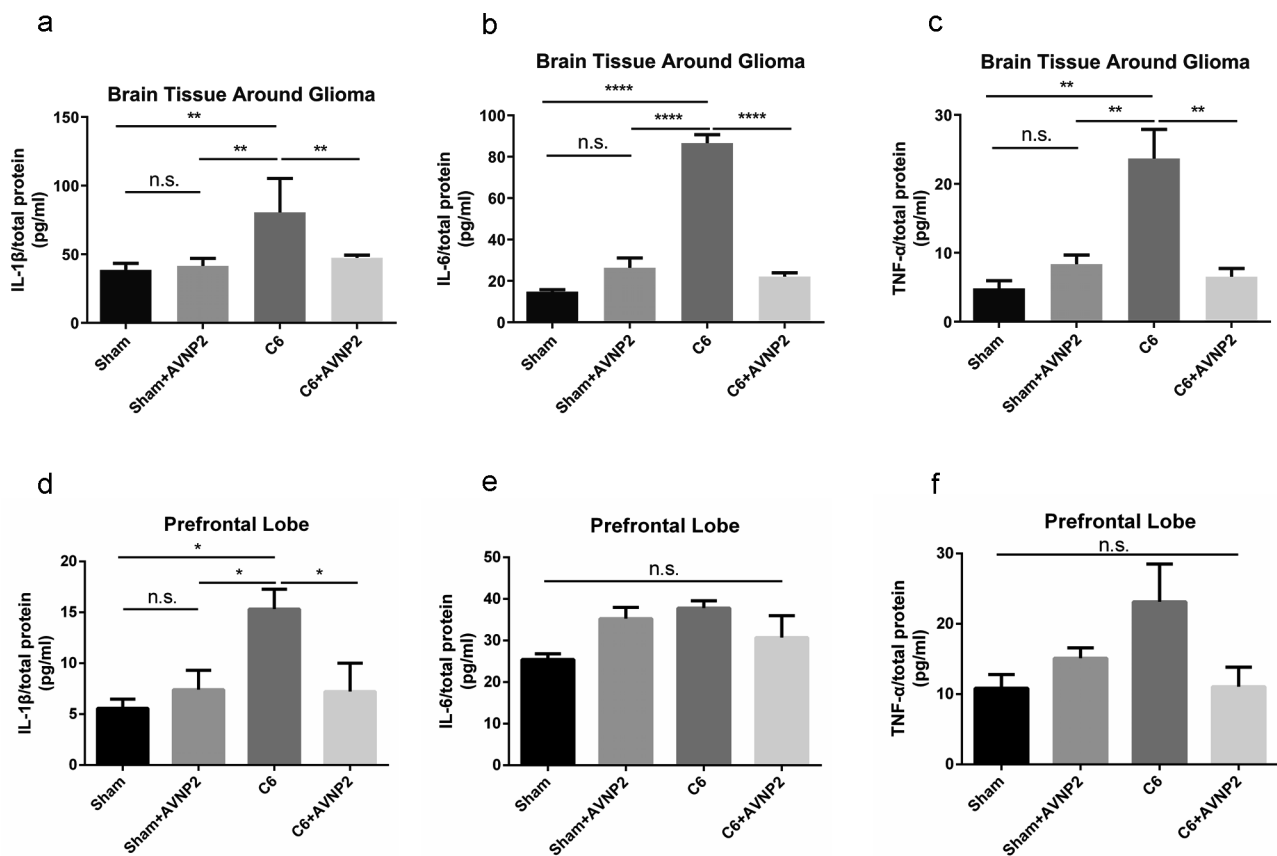


Fig. 11. The effects of AVNP2 administration on pro-inflammation-related protein measured by ELISA test. The ELISA test showed that the levels of IL-1 β , IL-6 and TNF- α from brain tissue around glioma and prefrontal lobe of rats of C6 group were increased significantly compared with all other groups (Fig. 11a–c, ** $P < 0.01$, **** $P < 0.0001$), no significant difference was found between Sham group and Sham + AVNP2 group (Fig. 11a–c, $P > 0.05$). The level of IL-1 β from prefrontal lobe of rats of C6 group was increased significantly compared with all other groups (Fig. 11d * $P < 0.05$), no significant difference was found between Sham group and Sham + AVNP2 group (Fig. 11d, $P > 0.05$). The levels of IL-6 and TNF- α from prefrontal lobe of rats showed no statistical difference among four groups (Fig. 11e, f $P > 0.05$). Data are expressed as mean \pm SEM, $n = 4$ per group, * $P < 0.05$, ** $P < 0.01$, **** $P < 0.0001$.

quercetin to modulate inflammation in the microglia and inhibit the proliferation of gliomas (da Silva et al., 2019).

Moreover, the inflammatory response could also be reflected by COX-2, iNOS and VEGF, one of the most vital known pro-angiogenic factors. We tested them in peri-tumour tissue. They have been claimed by considerable studies to be inextricably linked with glioblastoma (Myung et al., 2010; D'Alessandris et al., 2015). They affected the genesis of glioma and enhanced multifaceted biological capabilities by promoting angiogenesis and prognosis (Hara and Okayasu, 2004). Western blotting assay of COX-2, iNOS and VEGF did not totally prove the anti-angiogenesis function of AVNP2 on gliomas but gave us a hint, which needs to be investigated deeper by means of ELISA and the tubule formation test *in vivo* and *in vitro* (Chen et al., 2016). The activation or suppression of endothelial cells (ECs), which play an important part in tumour angiogenesis, are worthy of study and discussion too (Liu et al., 2018). In our experiment, results corresponded to the inflammation-related proteins mentioned before. With the administration of AVNP2, the levels of them were subdued in peri-tumour tissue. The down-regulation of inflammation-related proteins in peri-tumour tissue may be the reason for inhibition of TAMs by AVNP2, which are recruited by gliomas. However, it couldn't function as a protector in humans and secretes inflammatory cytokines to promote tumour cell proliferation inversely (Yang et al., 2017). Hwang JS *et al.* considered that IL-6, TNF- α , iNOS and COX-2 were glioma-secreted soluble factors that could stimulate the activation of TAMs (Hwang et al., 2016).

Up to now, the TME, especially tumour associated inflammation and the interaction between tumour cell and immune cells is not very clear. It is universally accepted that glioma-secreted soluble factors and TME-

secreted soluble factors all take part in the formation of the TME, and promote the proliferation of tumour cells (Barkal et al., 2019). What has been mentioned is that much research has focused on the micro-environment inside the glioma itself (Thorsson et al., 2018; Platten et al., 2018). However, peri-tumour inflammation is worth observing too, which happens in the normal brain region and directly influences normal brain function. Many years ago, some researchers and clinicians found patients diagnosed with cancer would suffer from psychiatric disorders, especially brain tumours. At the time, psychiatric disorders were partly blamed on the "paraneoplastic syndrome" (Benros et al., 2009; Dalton et al., 2009). Paraneoplastic syndromes are referred to as symptom complexes that occur in patients with cancer that cannot be readily explained by local or distant spread of the tumour. Nowadays, with a deeper understanding of the biological characteristics of gliomas, researchers have found that the interaction between gliomas and nerve cells was much more complex than we thought before. Tumour-derived factors, such as IL-6 and TNF- α , could implicate the hippocampus, prefrontal lobe and other brain regions (Walker Ii et al., 2017; Yang et al., 2014), and tumours could even form "synaptic-like" connections with nerve cells (Barria, 2019; Venkatesh et al., 2019). All these couldn't be explained just by the physical effect (i.e., mass effect of the brain tumour), but the biological effect (i.e., complex molecular interaction between the brain and tumour cells). Researchers have explored the relationship between tumours and cognition, and tumour-associated inflammation has attracted great interest. The pro-inflammatory and inflammatory factors, such as IL-6, IL-1 β and TNF- α , secreted by gliomas play a vital role in the implication that brain functional structures directly cause psychiatric disorders. In brief, the

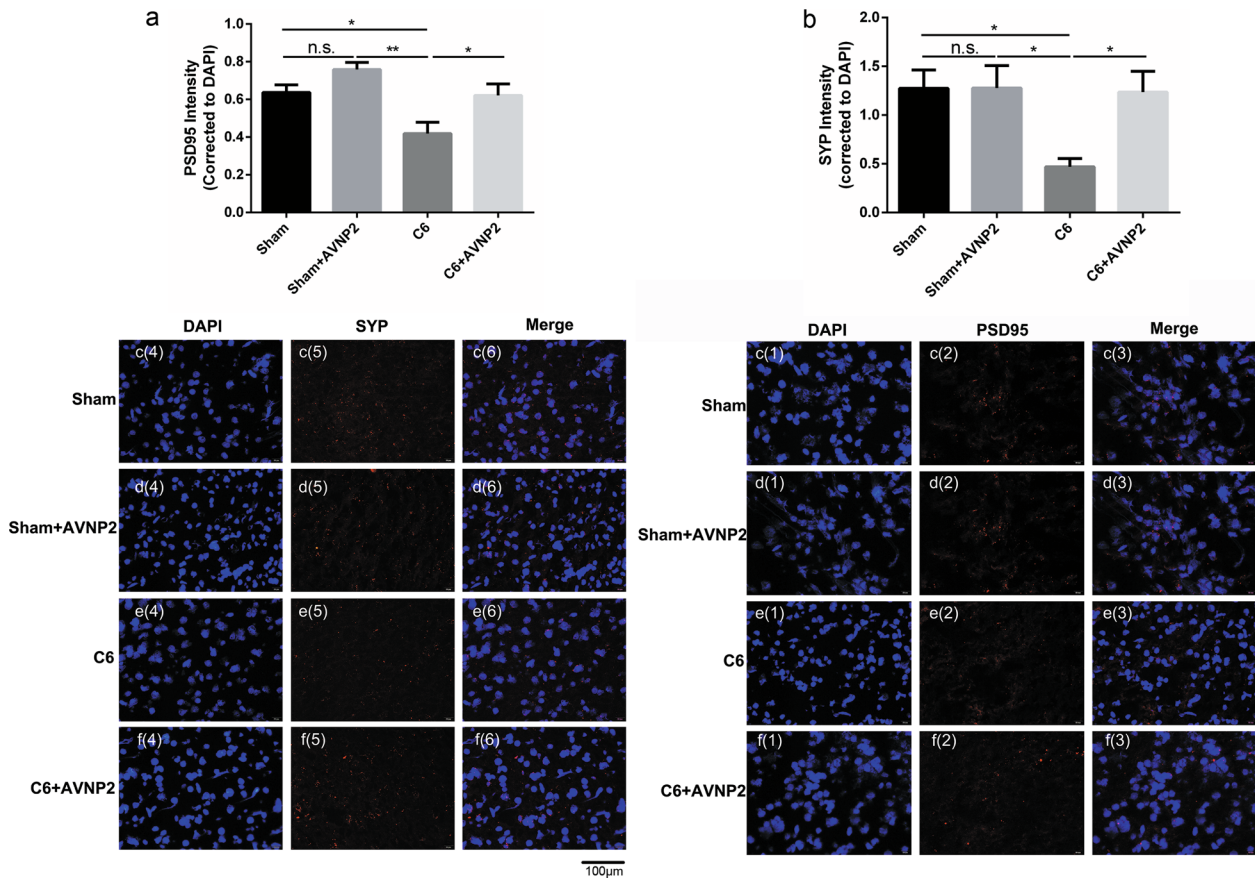


Fig. 12. The effects of AVNP2 administration on synaptic-related protein tested by Immunofluorescence staining test. Immunofluorescence staining test showed the protein intensity of PSD-95 (Fig. 12a) & SYP (Fig. 12b) across Sham, Sham + AVNP2, C6 and C6 + AVNP2 groups in cerebral cortex region. Images of immunofluorescence staining of PSD-95 [1:1000] (red) and SYP [1:1000] (red) with DAPI (blue) in Sham (Fig. 12c(1–6)), Sham + AVNP2 (Fig. 12d(1–6)), C6 (Fig. 12e(1–6)) and C6 + AVNP2 (Fig. 12f(1–6)) group. Quantitative intensity measurement showed a tendency of decrease in PSD-95 ($*P < 0.05$) and SYP ($*P < 0.05$) signal in C6 group compared with Sham group (Fig. 12a, b), and the reductions were removed in PSD-95 ($*P < 0.05$) and SYP ($*P < 0.05$) with AVNP2 administration in C6 + AVNP2 group (Fig. 12a, b). Data are expressed as mean \pm SEM, $n = 4$ per group, $*P < 0.05$, $**P < 0.01$.

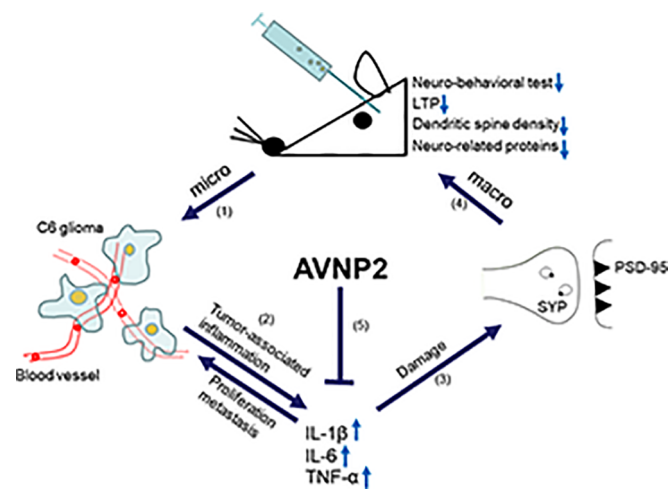


Fig. 13. Pattern diagram showed the multiple impacts of AVNP2 on C6 glioma model rats. Arrow (1) indicated that the research went from macro- into micro-dimensions and Arrow (4) indicated that the research went from micro- into macro- dimensions. The double sided Arrow (2) showed that glioma could induce inflammation by releasing pro-inflammation cytokines in peri-tumour tissues, and the pro-inflammation cytokines could promote glioma proliferation in return. Arrow (3) indicated that these cytokines could damage synaptic function. Arrow (5) indicated that AVNP2 could suppress the level of pro-inflammation cytokines and protects against cognitive impairment.

inflammation in the tumour associated environment has crucial effects on tumour proliferation and growth, as well as the normal functions of the brain. The better the inflammation is, the better the outcome (Fig. 13).

In this experiment, we used the classic glioma model- a C6 cell-based glioma rat model (Nagano et al., 1993; Chicoine and Silbergeld, 1995). Next, we measured the tumour volume of gliomas in C6 model rats (Braganhof et al., 2009). The volume obviously decreased after treatment with AVNP2, which proved that AVNP2 could indeed inhibit the growth of the tumour through modulation of the micro-environment. Many researchers have found that the tumour growth could be decreased by modulating inflammation (Ferrandon et al., 2015), which was also confirmed by our results. Besides, we obtained THz ATR to help us to define the margin of gliomas with imaging of freshly excised brain tissues with and without tumours at 2.52 THz. We chose it because THz ATR intensity imaging could be employed as a complementary technique, allowing surgeons to determine tumour regions with a label-free and diagnostic imaging method in real time. It has more important clinical significance than H&E staining (Reid et al., 2011; Parrott et al., 2011; Ji et al., 2016).

What should not be neglected is that emotional abnormalities and cognitive changes during the course of disease are among the various factors leading to cognitive impairment and immune and inflammatory factors play a key part. In our previous experiments, it was confirmed that cognitive abnormalities of glioma model rats occurred (Wang et al., 2011), which was the same in our preliminary work. Increasing studies have also shown that the release of inflammatory factors and activation

of related signalling pathways promote cognitive impairment in patients with brain tumours (Mostofa et al., 2017).

Campos-Pires et al explored the relationship between chronic neuro-inflammation and survival after traumatic brain injury in mice (Campos-Pires et al., 2019). The role of inflammation in Alzheimer disease (AD) and some psychological disorders has been studied much deeper than in other fields (Heppner et al. et al., 2015; Murata et al., 2020). Walker et al. found that cancer-induced systematic inflammation played an important role in cognitive impairment (Walker et al., 2018). The brain tumour induced inflammation, especially in the peri-tumour brain region, has resemblances with these. In this study, we suppressed the inflammation induced by gliomas, so we inferred that the cognition level of C6-bearing rats can be improved by AVNP2 administration. We implemented several of the following approaches: neuro-related proteins, staining of dendritic spines, electrophysiology tests and behavioural experiments, from the micro- to the macro-level, to evaluate the cognition level all-around.

Researches have proved the relationship between inflammation and both SYP and PSD-95. Inflammation could decrease the levels of SYP and PSD-95 (Yang et al., 2018) (Zong et al., 2012), but few have gone deeper into the tumour-induced inflammation. Hao et al found that C6 gliomas could lead to down-regulation of SYP, but no significant difference was found in the expression of PSD-95 (Hao et al., 2018). However, in our experiment, SYP and PSD-95 were both down-regulated in C6-bearing rats by the Western blotting assay and immunofluorescence staining test respectively, while the AVNP2 could reverse this by suppressing the pro-inflammation cytokines level, which were confirmed by Western blotting assay and ELISA test respectively. We considered that the different results happened because of the different experimental design. In Hao's experiment, the interval between C6 cell xenograft with tumour specimen collection was five days, however, in our experiment, the interval was eight days. We could reasonably assume that SYP is more sensitive to damage from inflammation than PSD-95. As shown in the immunofluorescence staining test, the degree of decrease with SYP was larger than PSD-95, and this was correlated with results of Western blotting. These synaptic plasticity-related molecules explained the improvement of neurocognitive and learning-memory function in rats with gliomas on the micro-level, which indicated that AVNP2 could inhibit the biological functions of gliomas by inhibiting inflammation and angiogenesis, thus enhancing the cognitive levels of GBM model rats.

In order to know the cognitive function at a histological level, we performed Golgi-cox staining. Firstly, in our experiment, the results apparently showed that AVNP2 could increase dendritic spine density in the hippocampus and further enhance the learning-memory ability of glioma model rats. Secondly, we confirmed the improved inflammation reaction in the same local tissue. Inflammation induces oedema and local hypertension, all of which could damage the dendritic spines. Decades ago, researchers found significant pathological changes in peritumour brain tissue, such as swollen dendrites, disarray of microtubules and decreased dendritic spine density. However, due to incomprehension of the neuro-immune system, no one had related these to tumour associated inflammation in local tissue (Spacek, 1987). This time, we inferred that AVNP2 improved cognitive function on a histological level (indirectly) by suppressing the tumour-associated inflammation in local areas. With the administration of AVNP2, the inflammation was controlled and injury to the hippocampus was relieved.

Accordingly, LTP was measured in the present study. We know that the slopes of fEPSPs have a positive correlation with synaptic transmission and memory in physiology. The LTP measurements in this study were consistent with the performance of memory, which was in line with our previous "microcosmic" results. The negative effect, tumour associated inflammation, on LTP was apparently impeded by the administration of AVNP2, which suggested that synaptic plasticity was remarkably enhanced in the hippocampus after modulating the level of tumour associated inflammation. In a word, the synaptic function of the

hippocampus was significantly improved after treatment with AVNP2 in glioma model rats. What's more, the C6-bearing rats performed better than rats without proper treatment in both the OFT and the NORT, which indicated the cognitive impairment caused by gliomas was ameliorated by AVNP2 on a behavioural test level.

5. Conclusion

In summary, our results indicated that AVNP2 not only depressed the local inflammation and angiogenesis in peri-tumour tissue but also inhibited the growth of gliomas in *in vivo* animal tests. We obtained gross tumour specimens and calculated the tumour volume reduction and used THz ATR imaging to identify the margins of gliomas. Our work indicated that AVNP2 could modulate tumour-associated inflammation, depress the size of gliomas and eventually alleviate the cognitive levels of C6-bearing rats. Our results also demonstrated an important and significant enlightenment from a preclinical and clinical medicine perspective for further research into cancer solutions.

Conflict of interest

The authors declare that they have no conflict of interest.

Acknowledgment

This work was supported by the National Natural Science Foundation of China (81771979).

References

- Zong, H., Verhaak, R.G., Canoll, P., 2012. The cellular origin for malignant glioma and prospects for clinical advancements. *Expert Rev. Mol. Diagn.* 12 (4), 383–394.
- Ohgaki, H., Kleihues, P., 2005. Epidemiology and etiology of gliomas. *Acta Neuropathol.* 109 (1), 93–108.
- Graus, F., et al., 2013. Patterns of care and outcome for patients with glioblastoma diagnosed during 2008–2010 in Spain. *Neuro Oncol.* 15 (6), 797–805.
- Tanaka, S., et al., 2013. Presentation, management, and outcome of newly diagnosed glioblastoma in elderly patients. *J. Neurosurg.* 118 (4), 786–798.
- Stupp, R., et al., 2017. Effect of tumor-treating fields plus maintenance temozolomide vs maintenance temozolomide alone on survival in patients with glioblastoma: a randomized clinical trial. *JAMA* 318 (23), 2306–2316.
- Okada, M., Miyake, K., Tamiya, T., 2017. Glioblastoma treatment in the elderly. *Neurol. Med. Chir. (Tokyo)* 57 (12), 667–676.
- Stupp, R., et al., 2009. Effects of radiotherapy with concomitant and adjuvant temozolomide versus radiotherapy alone on survival in glioblastoma in a randomised phase III study: 5-year analysis of the EORTC-NCIC trial. *Lancet Oncol.* 10 (5), 459–466.
- Solanki, C., et al., 2017. Impairments in quality of life and cognitive functions in long-term survivors of glioblastoma. *J. Neurosci. Rural Pract.* 8 (2), 228–235.
- Wang, Y.Y., et al., 2011. Impaired hippocampal synaptic plasticity in C6 glioma-bearing rats. *J. Neurooncol.* 103 (3), 469–477.
- Weitzner, M.A., Meyers, C.A., 1997. Cognitive functioning and quality of life in malignant glioma patients: a review of the literature. *Psychooncology* 6 (3), 169–177.
- Van Dyk, K., Ganz, P.A., 2019. The inflammation complication: New evidence in cancer-related cognitive impairment. *Brain Behav. Immun.* 81, 6–7.
- Crossen, J.R., et al., 1994. Neurobehavioral sequelae of cranial irradiation in adults: a review of radiation-induced encephalopathy. *J. Clin. Oncol.* 12 (3), 627–642.
- Janelsins, M.C., et al., 2011. An update on cancer- and chemotherapy-related cognitive dysfunction: current status. *Semin. Oncol.* 38 (3), 431–438.
- Vecht, C., et al., 2017. Seizures and anticonvulsants in brain tumours: frequency, mechanisms and anti-epileptic management. *Curr. Pharm. Des.* 23 (42), 6464–6487.
- Jacob, J., et al., 2018. Cognitive impairment and morphological changes after radiation therapy in brain tumors: a review. *Radiother. Oncol.* 128 (2), 221–228.
- Williams, C.N., et al., 2015. Hyponatremia and poor cognitive outcome following pediatric brain tumor surgery. *J. Neurosurg. Pediatr.* 15 (5), 480–487.
- Quant, E.C., et al., 2009. Role of a second chemotherapy in recurrent malignant glioma patients who progress on bevacizumab. *Neuro Oncol.* 11 (5), 550–555.
- Froklage, F.E., et al., 2014. Central neurotoxicity of standard treatment in patients with newly-diagnosed high-grade glioma: a prospective longitudinal study. *J. Neurooncol.* 116 (2), 387–394.
- Hilverda, K., et al., 2010. Cognitive functioning in glioblastoma patients during radiotherapy and temozolomide treatment: initial findings. *J. Neurooncol.* 97 (1), 89–94.
- Noy, R., Pollard, J.W., 2014. Tumor-associated macrophages: from mechanisms to therapy. *Immunity* 41 (1), 49–61.
- Wu, S.Y., Watabe, K., 2017. The roles of microglia/macrophages in tumor progression of brain cancer and metastatic disease. *Front. Biosci. (Landmark Ed.)* 22, 1805–1829.
- Sorensen, M.D., et al., 2018. Tumour-associated microglia/macrophages predict poor

- prognosis in high-grade gliomas and correlate with an aggressive tumour subtype. *Neuropathol. Appl. Neurobiol.* 44 (2), 185–206.
- Graf, M.R., et al., 2002. Irradiated tumor cell vaccine for treatment of an established glioma. I. Successful treatment with combined radiotherapy and cellular vaccination. *Cancer Immunol. Immunother.* 51 (4), 179–189.
- Mineharu, Y., et al., 2011. Engineering the brain tumor microenvironment enhances the efficacy of dendritic cell vaccination: implications for clinical trial design. *Clin. Cancer Res.* 17 (14), 4705–4718.
- Mostofa, A.G., et al., 2017. The process and regulatory components of inflammation in brain oncogenesis. *Biomolecules* 7 (2).
- McFarland, B.C., et al., 2013. NF-kappaB-induced IL-6 ensures STAT3 activation and tumor aggressiveness in glioblastoma. *PLoS One* 8 (11), e78728.
- Myung, J., et al., 2010. Snail and Cox-2 expressions are associated with WHO tumor grade and survival rate of patients with gliomas. *Neuropathology* 30 (3), 224–231.
- Cheong, Y.K., et al., 2017. Characterisation of the chemical composition and structural features of novel antimicrobial nanoparticles. *Nanomaterials* 7(7).
- Ren, G., 2010. **Antiviral nanoparticles.**
- Ren, G., 2013. **Antiviral nanoparticles.**
- Yang, Z., et al., 2010. A review of nanoparticle functionality and toxicity on the central nervous system. *J. R. Soc. Interface* 7 (Suppl. 4), S411–S422.
- Ren, G., et al., 2009. Characterisation of copper oxide nanoparticles for antimicrobial applications. *Int. J. Antimicrob. Agents* 33 (6), 587–590.
- Bankier, C., et al., 2018. A comparison of methods to assess the antimicrobial activity of nanoparticle combinations on bacterial cells. *PLoS One* 13 (2).
- Wan, G., et al., 2016. Effects of silver nanoparticles in combination with antibiotics on the resistant bacteria *Acinetobacter baumannii*. *Int. J. Nanomed.* 11, 3789–3800.
- Nan, L., et al., 2016. Antibacterial performance of Cu-bearing stainless steel against *Staphylococcus aureus* and *Pseudomonas aeruginosa* in Whole Milk. *J. Mater. Sci. Technol.* 32 (5), 445–451.
- Nan, L., Yang, K., Ren, G., 2015. Anti-biofilm formation of a novel stainless steel against *Staphylococcus aureus*. *Mater. Sci. Eng. C* 51, 356–361.
- Ren, L., et al., 2015. Determination of Cu²⁺ ions release rate from antimicrobial copper bearing stainless steel by joint analysis using ICP-OES and XPS. *Mater. Technol.* 30 (B2), B86–B89.
- Ren, L., et al., 2016. A novel coping metal material CoCrCu alloy fabricated by selective laser melting with antimicrobial and antibiofilm properties. *Mater. Sci. Eng. C* 67, 461–467.
- He, Y., et al., 2018. High-energy and ultra-wideband tunable terahertz source with DAST crystal via difference frequency generation. *Appl. Phys. B* 124 (1), 16.
- Sim, Y.C., et al., 2013. Terahertz imaging of excised oral cancer at frozen temperature. *Biomed. Opt. Express* 4 (8), 1413–1421.
- Woodward, R.M., et al., 2003. Terahertz pulse imaging of ex vivo basal cell carcinoma. *J. Invest. Dermatol.* 120 (1), 72–78.
- Reid, C.B., et al., 2011. Terahertz pulsed imaging of freshly excised human colonic tissues. *Phys. Med. Biol.* 56 (14), 4333.
- Park, J.Y., et al., 2017. Terahertz imaging of metastatic lymph nodes using spectroscopic integration technique. *Biomed. Opt. Express* 8 (2), 1122–1129.
- Oh, S.J., et al., 2014. Study of freshly excised brain tissues using terahertz imaging. *Biomed. Opt. Express* 5 (8), 2837–2842.
- Meng, K., et al., 2014. Terahertz pulsed spectroscopy of paraffin-embedded brain glioma. *J. Biomed. Opt.* 19 (7), 077001.
- Wu, L., et al., 2019. Study of in vivo brain glioma in a mouse model using continuous-wave terahertz reflection imaging. *Biomed. Opt. Express* 10 (8), 3953–3962.
- Ovais, M., Guo, M., Chen, C., 2019. Tailoring nanomaterials for targeting tumor-associated macrophages. *Adv. Mater.*, e1808303.
- Gong, T., et al., 2019. Spontaneously formed porous structure and M1 polarization effect of Fe₃O₄ nanoparticles for enhanced antitumor therapy. *Int. J. Pharm.* 559, 329–340.
- Reichel, D., Tripathi, M., Perez, J.M., 2019. Biological effects of nanoparticles on macrophage polarization in the tumor microenvironment. *Nanotheranostics* 3 (1), 66–88.
- d'Isa, R., Brambilla, R., Fasano, S., 2014. Behavioral methods for the study of the Ras-ERK pathway in memory formation and consolidation: passive avoidance and novel object recognition tests. *Methods Mol. Biol.* 1120, 131–156.
- Sholl, D.A., 1953. Dendritic organization in the neurons of the visual and motor cortices of the cat. *J. Anat.* 87 (4), 387–406.
- Sorra, K.E., Harris, K.M., 2000. Overview on the structure, composition, function, development, and plasticity of hippocampal dendritic spines. *Hippocampus* 10 (5), 501–511.
- Zhang, H., et al., 2017. Prenatal stress-induced impairments of cognitive flexibility and bidirectional synaptic plasticity are possibly associated with autophagy in adolescent male-offspring. *Exp. Neurol.* 298 (Pt A), 68–78.
- Ostrom, Q.T., et al., 2015. CBTRUS statistical report: primary brain and central nervous system tumors diagnosed in the United States in 2008–2012. *Neuro Oncol.* 17 (Suppl. 4), iv1–iv62.
- Saalik, P., et al., 2019. Peptide-guided nanoparticles for glioblastoma targeting. *J. Control. Release* 308, 109–118.
- Del Sol-Fernandez, S., Portilla-Tundidor, Y., Gutierrez, L., 2019. Flower-like Mn-doped magnetic nanoparticles functionalized with alpha5beta3-integrin-ligand to efficiently induce intracellular heat after alternating magnetic field exposition triggering glioma cell death. *ACS Appl. Mater. Interfaces* 11 (30), 26648–26663.
- Yu, M., et al., 2019. D-17 peptide-modified pegylated bilirubin nanoparticles loaded with cediranib and paclitaxel for antiangiogenesis and chemotherapy of Glioma. *ACS Appl. Mater. Interfaces* 11 (1), 176–186.
- Liang, J., et al., 2018. Natural brain penetration enhancer-modified albumin nanoparticles for glioma targeting delivery. *ACS Appl. Mater. Interfaces* 10 (36), 30201–30213.
- Zhu, C., et al., 2017. The contribution of tumor-associated macrophages in glioma neo-angiogenesis and implications for anti-angiogenic strategies. *Neuro Oncol.* 19 (11), 1435–1446.
- Shan, Y., et al., 2015. Role of IL-6 in the invasiveness and prognosis of glioma. *Int. J. Clin. Exp. Med.* 8 (6), 9114–9120.
- Lang, F.F., et al., 2018. Phase I study of DNX-2401 (Delta-24-RGD) oncolytic adenovirus: replication and immunotherapeutic effects in recurrent malignant glioma. *J. Clin. Oncol.* 36 (14), 1419–1427.
- Thompson, E.M., et al., 2016. Prognostic value of medulloblastoma extent of resection after accounting for molecular subgroup: a retrospective integrated clinical and molecular analysis. *Lancet Oncol.* 17 (4), 484–495.
- Zou, C., et al., 2019. CD48 is a key molecule of immunomodulation affecting prognosis in glioma. *Onco Targets Ther.* 12, 4181–4193.
- Wang, H., et al., 2009. Targeting interleukin 6 signaling suppresses glioma stem cell survival and tumor growth. *Stem Cells* 27 (10), 2393–2404.
- da Silva, A.B., et al., 2019. The flavonoid rutin and its aglycone quercetin modulate the microglia inflammatory profile improving anti-glioma activity. *Brain Behav. Immun.*
- D'Alessandris, Q.G., et al., 2015. VEGF isoforms as outcome biomarker for anti-angiogenic therapy in recurrent glioblastoma. *Neurology* 84 (18), 1906–1908.
- Hara, A., Okayasu, I., 2004. Cyclooxygenase-2 and inducible nitric oxide synthase expression in human astrocytic gliomas: correlation with angiogenesis and prognostic significance. *Acta Neuropathol.* 108 (1), 43–48.
- Chen, L., et al., 2016. Upregulation of miR-107 inhibits glioma angiogenesis and VEGF expression. *Cell. Mol. Neurobiol.* 36 (1), 113–120.
- Liu, T., et al., 2018. PDGF-mediated mesenchymal transformation renders endothelial resistance to anti-VEGF treatment in glioblastoma. *Nat. Commun.* 9 (1), 3439.
- Yang, J., et al., 2017. MiR-15a/16 deficiency enhances anti-tumor immunity of glioma-infiltrating CD8⁺ T cells through targeting. *mTOR* 141 (10), 2082–2092.
- Hwang, J.S., et al., 2016. Glioma-secreted soluble factors stimulate microglial activation: the role of interleukin-1beta and tumor necrosis factor-alpha. *J. Neuroimmunol.* 298, 165–171.
- Barkal, A.A., et al., 2019. CD24 signalling through macrophage Siglec-10 is a target for cancer immunotherapy. *Nature* 572 (7769), 392–396.
- Thorsson, V., et al., 2018. The immune landscape of cancer. *Immunity* 48 (4), 812–830.e14.
- Platten, M., 2018. T cells engineered to home in on brain cancer. *Nature* 561 (7723), 319–320.
- Benros, M.E., et al., 2009. Psychiatric disorder as a first manifestation of cancer: a 10-year population-based study. *Int. J. Cancer* 124 (12), 2917–2922.
- Dalton, S.O., et al., 2009. Risk for hospitalization with depression after a cancer diagnosis: a nationwide, population-based study of cancer patients in Denmark from 1973 to 2003. *J. Clin. Oncol.* 27 (9), 1440–1445.
- Walker li, W.H., et al., 2017. Mammary tumors induce central pro-inflammatory cytokine expression, but not behavioral deficits in Balb/C mice. *Sci. Rep.* 7 (1), 8152.
- Yang, M., et al., 2014. Hippocampal dysfunctions in tumor-bearing mice. *Brain Behav. Immun.* 36, 147–155.
- Barria, A., 2019. Dangerous liaisons as tumour cells form synapses with neurons. *Nature* 573 (7775), 499–501.
- Venkatesh, H.S., et al., 2019. Electrical and synaptic integration of glioma into neural circuits. *Nature* 573 (7775), 539–545.
- Nagano, N., et al., 1993. Invasion of experimental rat brain tumor: early morphological changes following microinjection of C6 glioma cells. *Acta Neuropathol.* 86 (2), 117–125.
- Chicoine, M.R., Silbergeld, D.L., 1995. Invading C6 glioma cells maintaining tumor-igenicity. *J. Neurosurg.* 83 (4), 665–671.
- Braganhol, E., et al., 2009. Selective NTPDase2 expression modulates in vivo rat glioma growth. *Cancer Sci.* 100 (8), 1434–1442.
- Ferrando, S., et al., 2015. Telomerase inhibition improves tumor response to radiotherapy in a murine orthotopic model of human glioblastoma. *Mol. Cancer* 14, 134.
- Parrott, E.P., et al., 2011. Terahertz pulsed imaging in vivo: measurements and processing methods. *J. Biomed. Opt.* 16 (10), 106010.
- Ji, Y.B., et al., 2016. Terahertz reflectometry imaging for low and high grade gliomas. *Sci. Rep.* 6, 36040.
- Campos-Pires, R., et al., 2019. Xenon improves long-term cognitive function, reduces neuronal loss and chronic neuroinflammation, and improves survival after traumatic brain injury in mice. *Br. J. Anaesth.* 123 (1), 60–73.
- Heppner, F.L., Ransohoff, R.M., Becher, B., 2015. Immune attack: the role of inflammation in Alzheimer disease. *Nat. Rev. Neurosci.* 16 (6), 358–372.
- Murata, S., et al., 2020. Effects of adjunctive inflammatory modulation on IL-1beta in treatment resistant bipolar depression. *Brain Behav. Immun.*
- Walker, A.K., et al., 2018. Low dose aspirin blocks breast cancer-induced cognitive impairment in mice. *PLoS One* 13 (12), e0208593.
- Yang, L., et al., 2018. Fluoride activates microglia, secretes inflammatory factors and influences synaptic neuron plasticity in the hippocampus of rats. *Neurotoxicology* 69, 108–120.
- Hao, S., et al., 2018. AG-1031 and AG-1503 improve cognitive deficits by promoting apoptosis and inhibiting autophagy in C6 glioma model rats. *Brain Res.* 1699, 1–8.
- Spacek, J., 1987. Ultrastructural pathology of dendritic spines in epitemorous human cerebral cortex. *Acta Neuropathol.* 73 (1), 77–85.